


Ectopic expression of a rice plasma membrane intrinsic protein (OsPIP1;3) promotes plant growth and water uptake

Siyu Liu¹, Tatsuya Fukumoto², Patrizia Gena³, Peng Feng¹, Qi Sun¹, Qiang Li¹, Tadashi Matsumoto², Toshiyuki Kaneko⁴, Hang Zhang¹, Yao Zhang⁵, Shihua Zhong⁶, Weizhong Zeng⁷, Maki Katsuhara⁴, Yoshichika Kitagawa², Aoxue Wang⁵, Giuseppe Calamita^{3,*} and Xiaodong Ding^{1,*} 

¹Key Laboratory of Agricultural Biological Functional Genes, Northeast Agricultural University, Harbin 150030, China,

²Graduate School of Bioresource Sciences, Akita Prefectural University, Akita 010-0195, Japan,

³Department of Biosciences, Biotechnologies and Biopharmaceutics, University of Bari 'Aldo Moro', Bari, Italy,

⁴Research Institute for Bioresources, Okayama University, Kurashiki 710-0046, Japan,

⁵College of Horticulture, Northeast Agricultural University, Harbin 150030, China,

⁶Department of Biochemistry, the University of Texas Southwestern Medical Center, Dallas, TX 75390, USA, and

⁷Department of Biophysics, the University of Texas Southwestern Medical Center, Dallas, TX 75390, USA

Received 14 November 2018; revised 9 November 2019; accepted 9 December 2019.

*For correspondence (e-mail xiaodong.ding@neau.edu.cn; giuseppe.calamita@uniba.it).

SUMMARY

Plasma membrane intrinsic proteins (PIPs) are known to be major facilitators of the movement of a number of substrates across cell membranes. From a drought-resistant cultivar of *Oryza sativa* (rice), we isolated an *OsPIP1;3* gene single-nucleotide polymorphism (SNP) that is mostly expressed in rice roots and is strongly responsive to drought stress. Immunocytochemistry showed that *OsPIP1;3* majorly accumulated on the proximal end of the endodermis and the cell surface around the xylem. Expression of *GFP-OsPIP1;3* alone in *Xenopus* oocytes or rice protoplasts showed *OsPIP1;3* mislocalization in the endoplasmic reticulum (ER)-like neighborhood, whereas co-expression of *OsPIP2;2* recruited *OsPIP1;3* to the plasma membrane and led to a significant enhancement of water permeability in oocytes. Moreover, reconstitution of 10×His-*OsPIP1;3* in liposomes demonstrated water channel activity, as revealed by stopped-flow light scattering. Intriguingly, by patch-clamp technique, we detected significant NO₃⁻ conductance of *OsPIP1;3* in mammalian cells. To investigate the physiological functions of *OsPIP1;3*, we ectopically expressed the *OsPIP1;3* gene in *Nicotiana benthamiana* (tobacco). The transgenic tobacco plants exhibited higher photosynthesis rates, root hydraulic conductivity (Lp_r) and water-use efficiency, resulting in a greater biomass and a higher resistance to water deficit than the wild-type did. Further experiments suggested that heterologous expression of *OsPIP1;3* in cyanobacterium altered bacterial growth under different conditions of CO₂ gas supply. Overall, besides shedding light on the multiple functions played by *OsPIP1;3*, this work provides insights into the translational value of plant AQPs.

Keywords: aquaporin, water, nitrate, carbon dioxide, permeability, hydraulic conductivity, membrane transport, plant growth.

INTRODUCTION

Membrane intrinsic proteins (MIPs) constitute an ancient family of proteinaceous channels widely distributed in all three kingdoms of life (eukarya, bacteria and archaea). MIPs are small proteins with six transmembrane (TM) α -helices connected by five loops as well as cytosol-localized N and C termini. Aquaporins (AQPs) belong to the MIP superfamily and function as channel proteins known for their abilities to conduct water and/or small molecules

across biological membranes. Since the first AQP was discovered (Preston *et al.*, 1992) numerous homologs have been identified and characterized from microorganisms, plants and animals, including humans. Orthodox AQPs act as filters that stringently exclude the passage of charged molecules and solutes larger than water. As a result of long-term evolution, however, different organisms have evolved and now possess different cell organization and physiological features. For example, photoautotrophic

plants, some photoautotrophic microorganisms and heterotrophic animals possess distinct AQPs, with different substrate specificities and channel activities (Ishibashi *et al.*, 2017).

Aquaporin substrate specificity, expression and localization varies among the different AQP members from different species. Human AQP1 was the first cloned AQP to transport water (Preston *et al.*, 1992) and CO₂ (Nakhoul *et al.*, 1998) in *Xenopus* oocytes across the cell membrane, and human AQP3 was discovered to be permeable to glycerol and urea (Echevarría *et al.*, 1996). The first work addressing plant AQPs led to the cloning of γ -TIP, a water-specific channel found in the vacuolar membrane of Arabidopsis (Maurel *et al.*, 1993). Thereafter, more plant water channel proteins were identified and characterized (reviewed by Kaldenhoff and Fischer, 2006; reviewed by Maurel *et al.*, 2008). In addition, many plant AQPs were found to have additional functions in transporting other small molecules, such as glycerol (Dean *et al.*, 1999), urea (Gaspar *et al.*, 2003), boron (Takano *et al.*, 2006), H₂O₂ (Rodrigues *et al.*, 2017), ammonia (Hwang *et al.*, 2010), CO₂ (Uehlein *et al.*, 2003) and O₂ (Zwiasek *et al.*, 2017). No NO₃⁻ permeability in plant AQPs except mammalian Aquaporin-6 (Ikeda *et al.*, 2002) has been reported, until now.

With the rapid development of DNA sequencing technology, many plant genomes have now been sequenced. Genomics data reveal that plants have greatly evolved and diversified, possessing many more AQP homologs than are found in other organisms, mostly because of their sessile nature in the face of ever-changing environmental conditions (Abascal *et al.*, 2014). For example, *Oryza sativa* (rice) has 34, Arabidopsis has 35, *Zea mays* (maize) has 43, *Glycine max* (soybean) has 72, and *Brassica oleracea* has 67 homologs (Deshmukh *et al.*, 2016). Based on their sequences and structures, plant AQPs are generally grouped into five subfamilies: NIP (similar to aquaglyceroporin of nitrogen-fixing bacteria of legume), PIP (plasma membrane intrinsic protein), SIP (small basic intrinsic protein), TIP (tonoplast intrinsic protein) and XIP (AQPs of unknown function). These AQPs localize in plasma membranes (PIPs and some NIPs), tonoplast (TIPs), endoplasmic reticulum (SIPs) and/or other subcellular compartments (Maurel *et al.*, 2015). The permeability of the different isoforms is directly or indirectly related to their specific physiological functions. Until now, huge progress has been made in the characterization of this family, allowing insights into their roles in the control of plant-environment relationships (Fox *et al.*, 2017). For example, ectopic expression of the *Malus domestica* (apple) *MdPIP1;3* gene in *Solanum lycopersicum* (tomato) enlarged fruit size and enhanced drought tolerance (Wang *et al.*, 2017a). Arabidopsis PIP1b overexpression in tobacco significantly increased plant growth, transpiration rate, stomatal density and photosynthetic efficiency (Aharon

et al., 2003), whereas overexpression of GsPIP2;1 from wild soybean in Arabidopsis attenuated the resistance to salt and dehydration (Wang *et al.*, 2015). Moreover, ectopic expression of a fungal aquaglyceroporin gene in tobacco improved water-use efficiency (WUE) and drought tolerance (Vieira *et al.*, 2017). On the other hand, tobacco NtAQP1 (NtPIP1) (Uehlein *et al.*, 2003) and cyanobacterial SsAqpZ (Ding *et al.*, 2013) were proven to help permeate CO₂ and thus enhanced plant and cyanobacterial photosynthesis. A recent study reported that the overexpression of rice aquaporin OsPIP1;2 improved yield by enhancing mesophyll CO₂ conductance and phloem sucrose transport (Xu *et al.*, 2019); however, the arguments about this aspect have continued over decades (Missner *et al.*, 2008).

Water deficit and drought stress can induce a series of plant responses, including leaf wilting, decreased photosynthesis and metabolic reactions, and oxidative damage in chloroplasts (Almeida-Rodriguez *et al.*, 2010). To tolerate these stresses, plants evolve various strategies, such as the adjustment of stomatal closure and hydraulic conductivity by altering turgor pressure in leaf and root cells, where AQPs may play important roles in regulating the trans-cellular transport of water (Maurel *et al.*, 2008).

Rice has 11 PIP isoforms, including three OsPIP1 and eight OsPIP2 members. Although systematic expression analyses have been conducted for the AQP family in rice (Nguyen *et al.*, 2013), their precise functions remain mostly elusive. Generally, the plant PIP2 group shows higher water permeability than the PIP1 group in *Xenopus* oocytes (Chaumont *et al.*, 2000). We have functionally characterized rice *OsPIP1;1* and *OsPIP1;3*, the overexpression of which enhanced plant salt and chilling tolerances, respectively (Matsumoto *et al.*, 2009; Liu *et al.*, 2013). Lian *et al.* (2004, 2006) observed that *OsPIP1;3* was strongly responsive to drought challenge and played pivotal role in drought avoidance in upland rice; however, the molecular mechanism of how *OsPIP1;3* functions in the plant physiological processes is largely unknown. In this work, we characterized a single-nucleotide polymorphism (SNP) of *OsPIP1;3* from a drought-resistant rice cultivar and unveiled its functions in promoting plant tolerance to water deficit and growth.

RESULTS

Comparison of *OsPIP1;3* sequences and expression pattern in rice

Although the water permeability of *OsPIP1;3* from a chilling-tolerant but drought-sensitive *O. sativa* L. spp. *japonica* cultivar has been characterized in *Xenopus* oocytes (Matsumoto *et al.*, 2009), the *OsPIP1;3* gene described in this work was isolated from a drought-tolerant *O. sativa* L. spp. *indica* cultivar. The alignment of *OsPIP1;3* sequences from the two subspecies indicates that the fragments in

their N-terminal tails have an eight-amino-acid difference, and that one glycine residue in the fifth TM domain of *OsPIP1;3* from the *indica* cultivar is missing (Figure S1), suggesting that SNPs of AQP genes are widely present in different species and ecological types of rice and may potentially contribute to functional diversity.

Total RNA from roots, shoots and leaves was extracted from 1-month-old rice seedlings (*O. sativa* L. spp. *indica* cv. Zhonghan 3) under favorable growth conditions and used for quantitative real-time PCR (qPCR) assays using the primers listed in Table S1. The data show that *OsPIP1;2* was ubiquitously expressed in the whole plants at lower levels, whereas *OsPIP1;1* had higher expression level in leaves than in roots. *OsPIP1;3* was mostly expressed in both leaves and roots, however, and *OsPIP2;2* was dominantly expressed in roots (Figure 1a). To investigate the response of *OsPIP1;3* to different environmental stimuli further, the rice seedlings were treated with 500 mM NaCl, 20% polyethylene glycol (PEG) or 4°C for 2 h and the total RNA from whole plants was extracted for qPCR assays. The results indicated that *OsPIP1;1* was significantly and specifically induced by PEG, chilling and salt, whereas *OsPIP1;3* was induced by drought and chilling but not by salt (Figure 1b). By using an anti-*OsPIP1;3*-specific antibody, the protein levels of endogenous *OsPIP1;3* in different rice tissues could be determined. The quantified protein levels were basically consistent with the transcript levels. Taken together, it is reasonable to state that *OsPIP1;3* is dominantly expressed in rice roots (Figure 1c, d).

Cellular and subcellular localization of *OsPIP1;3*

To assess the *in situ* localization of *OsPIP1;3*, we used an anti-*OsPIP1;3*-specific antibody to immunostain the endogenous *OsPIP1;3* protein in rice root tips. The immunoelectron microscopy data show that *OsPIP1;3* was mainly localized at the proximal end of the endodermis and the cell surface around the xylem (Figure S2a–c), suggesting that *OsPIP1;3* may play important roles in transporting water and other nutrients. As a negative control, no significant signal was detected from the root tip cells by staining with rabbit sera (Figure S2d).

To investigate the subcellular localization of *OsPIP1;3* further, *OsPIP1;3* and *OsPIP2;2* open reading frames (ORFs) were fused with genes coding for different fluorescent proteins, respectively. The plant transient expression constructs obtained were transformed into rice O.c. protoplasts. Single expression of EGFP-*OsPIP1;3* in the rice protoplasts resulted in the abnormal retention of GFP signal in ER-like membranes around the nucleus (Figure 2a, b), but the fluorescence of EGFP-*OsPIP2;2* was solely observed in the plasma membrane of rice protoplasts (Figure 2c,d). To examine whether the abnormal localization of EGFP-*OsPIP1;3* is altered by the interaction of other PIP

isoforms, we co-expressed EGFP-*OsPIP1;3* (green) with a small quantity of mDsRed-*OsPIP2;2* (red) in rice protoplasts. The resulting fluorescence patterns suggest that *OsPIP1;3* could be recruited to the plasma membrane by *OsPIP2;2* (Figure 2e–g).

In the animal *Xenopus* oocyte system, we expressed an equal quantity of EGFP-*OsPIP1;3* or EGFP-*OsPIP2;2* in oocytes and observed that the eggs injected with EGFP-*OsPIP1;3* showed a very weak GFP signal (Figure 2h), whereas the eggs injected with EGFP-*OsPIP2;2* showed a strong signal at the plasma membranes (Figure 2i). When co-expressing EGFP-*OsPIP1;3* with a small quantity of *OsPIP2;2*, however, we observed that the GFP signal was strongly re-localized to the plasma membrane (Figure 2j), implying that *OsPIP2;2* can recruit *OsPIP1;3* to the plasma membrane system, probably through a physical interaction.

Measurement of water permeability of *OsPIP1;3*

In order to determine the biophysical functions of *OsPIP1;3* from the rice *indica* cultivar, we expressed *OsPIP1;3* and/or *OsPIP2;2* in *Xenopus* oocytes to measure water permeability across the cell membrane. As shown in Figure 3(a), *OsPIP1;3* demonstrated almost negligible water channel activity no matter how much plasmid DNA was transformed, whereas *OsPIP2;2* demonstrated significant activity with a linear dose effect. *OsPIP1;3* exhibited significant channel activity in the presence of a small quantity of *OsPIP2;2* in *Xenopus* oocytes (Figure 3a), however, suggesting that both physical interaction and heterotetramerization among different PIP1 proteins are required for the synergistic effect on water permeability (Fetter *et al.*, 2004; Bienert *et al.*, 2018). The phenomenon of most PIP1 proteins failing to target to the plasma membrane and residing in intracellular membranes results from either missing plasma membrane trafficking signals or existing ER retention motifs (Chevalier and Chaumont, 2015).

To overcome the complexity of the oocyte system and to determine *OsPIP1;3* activity, independently from other factors, we produced and purified recombinant *OsPIP1;3* by an *Escherichia coli* system and reconstituted it into liposomes to measure the water permeability by a stopped-flow light-scattering approach (Liu *et al.*, 2013).

The *OsPIP1;3* ORF with a 10×His tag sequence at its 5' terminus was inserted into a prokaryotic expression vector. Owing to the failure of the target protein expression, the *OsPIP1;3* gene codons were optimized to maximize its expression in *E. coli*. The clear supernatants containing membrane fragments from the *E. coli* lysates were ultracentrifuged to pellet the cell membranes. As it is difficult to efficiently extract the TM proteins from the membrane pellets, we screened a series of distinct detergents to solubilize the recombinant *OsPIP1;3* protein out of the *E. coli* crude membrane fraction and found that a solubilization buffer containing 1.5% Fos-Choline 12 (FC12) or 4%

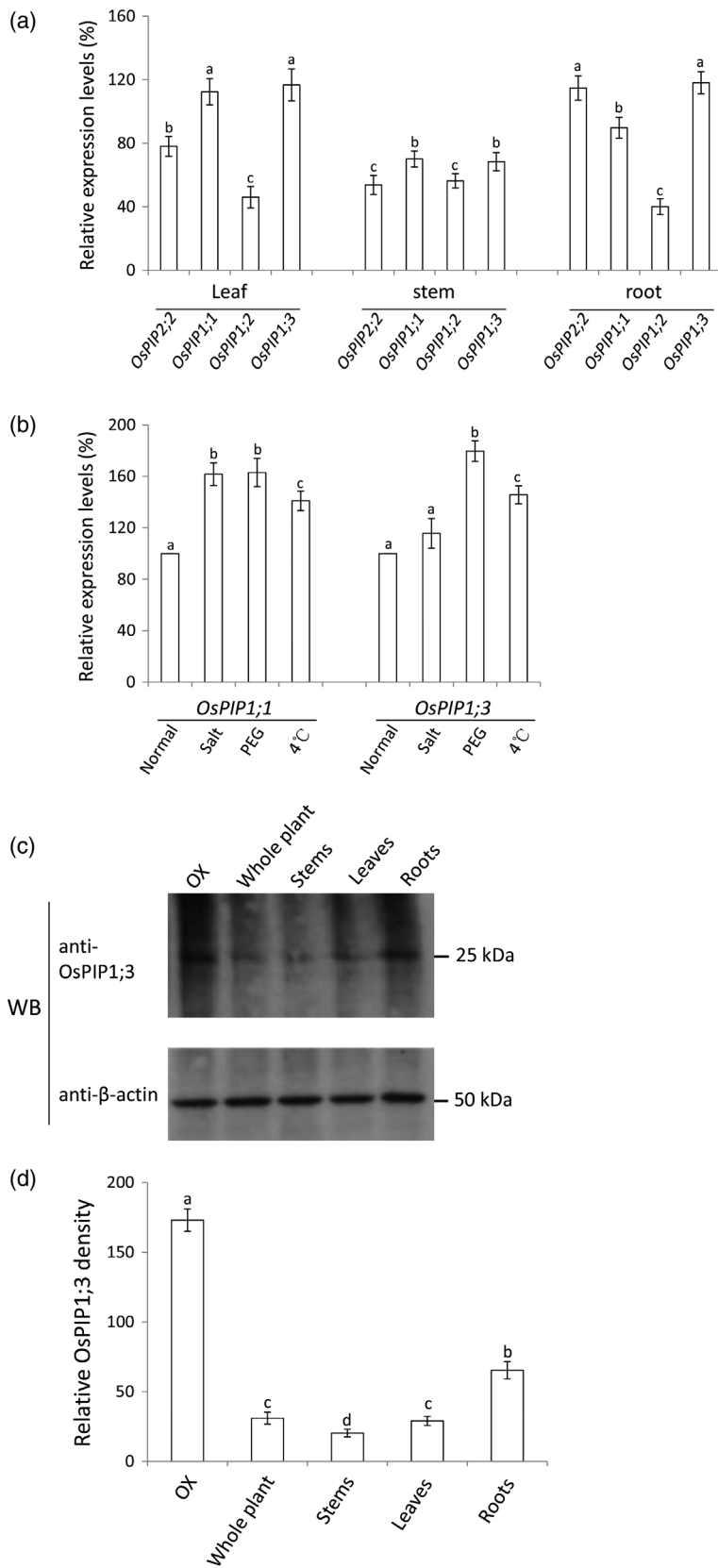


Figure 1. Expression patterns of rice *PIP1* genes. Total RNA and protein samples were extracted from *Oryza sativa* (rice) tissues for RT-qPCR and Western blotting analyses. (a) Analyses of the spatial expression of *PIP1* genes in rice tissues by RT-qPCR. (b) Responsive expression patterns of *PIP1* genes in roots to different environmental stimuli. The relative values were normalized by ubiquitin gene abundance. (c) Western blotting using anti-OsPIP1;3-specific antibody against protein lysates extracted from whole plant, stems, leaves and roots of the wild-type (WT) rice. OX is protein lysate from the OsPIP1;3-overexpression plant. (d) Relative abundance of OsPIP1;3 protein in rice tissues. Bars with different lowercase letters were significantly different (Duncan's multiple range test: $P < 0.05$).

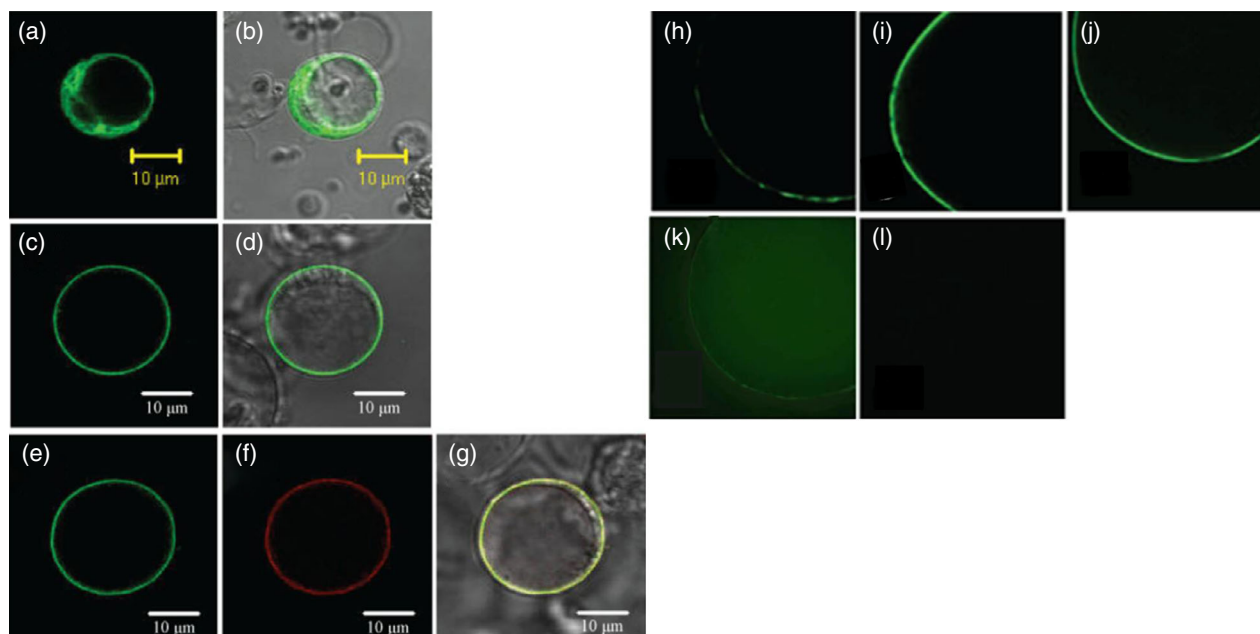


Figure 2. Subcellular localization of *OsPIP1;3* in *Oryza sativa* (rice) protoplasts and *Xenopus* oocytes.

Rice O.c. protoplasts were prepared and transformed with the following plasmids alone or plasmid combinations by the polyethylene glycol method: (a, b) EGFP-*OsPIP1;3* only; (c, d) EGFP-*OsPIP1;3* plus *OsPIP2;2*; and (e–g) EGFP-*OsPIP1;3* plus mDsRed-*OsPIP2;2*. At 16 h after DNA transformation, the images were taken by a laser scanning confocal microscope. *Xenopus* oocytes were prepared and injected with the following plasmids alone or plasmid combinations: (h) 25 ng of *PIP1;3*-EGFP cRNA; (i) 25 ng of *PIP2;2*-EGFP cRNA; (j) 25 ng of *PIP1;3*-EGFP cRNA and 3 ng of *PIP2;2* cRNA; (k) 25 ng of EGFP cRNA; (l) water. At 48 h after injection, the images were taken by a laser scanning confocal microscope.

perfluorooctanoic acid (PFO) detergent (lanes 8 and 9 in Figure S3a) could generate higher yields of soluble *OsPIP1;3* protein from membrane pellets. Subsequently, the 10×His-*OsPIP1;3* recombinant protein was then purified using nickel–nitrilotriacetic acid (Ni-NTA) columns. The protein samples obtained were resolved in sodium dodecyl sulfate polyacrylamide gel electrophoresis (SDS-PAGE) gels. Coomassie brilliant blue staining and Western blotting analyses using antibody against *OsPIP1;3* indicated that the recombinant *OsPIP1;3* was successfully expressed and purified with clear monomeric and dimeric bands (Figure S3b). A final quantity of 1.7 mg of purified 10×His-*OsPIP1;3* protein was obtained from 13 g of fresh *E. coli* crude proteins harvested from 10 L of *E. coli* culture. The purified 10×His-*OsPIP1;3* protein was reconstituted into liposome to generate proteoliposomes for the measurement of its water conducting activity. 10×His-*OsPIP1;3* activity was evaluated by stopped-flow light scattering after quickly exposing the proteoliposomes (versus control empty liposomes) to an osmotic upshock of 140 mOsm with the impermeant solute mannitol at 20°C. The coefficient of osmotic water permeability (P_f) of the 10×His-*OsPIP1;3* proteoliposomes was 62 $\mu\text{m sec}^{-1}$, significantly higher than that of the empty liposomes (8.6 $\mu\text{m sec}^{-1}$) (Figure 3b,c), indicating that 10×His-*OsPIP1;3* has functional water channel activity *in vitro*. To further confirm these results, we incubated the

proteoliposomes with 300 μM Hg^{2+} for 5 min and observed a pronounced reduction of water permeability. This inhibition could be partially alleviated by 15-min exposure to 10 mM β -mercaptoethanol, however, a reducing agent removing the Hg^{2+} bound to threonines and/or cysteines (Figure 3b,c), thereby confirming that *OsPIP1;3* is an active and *bona fide* water channel *in vitro*.

Measurement of nitrate permeability of *OsPIP1;3*

To determine whether *OsPIP1;3* has other permeable substrates besides water, we expressed *OsPIP1;3* in mammalian cells and detected its ion permeability by patch-clamp electrophysiological technique. The fluorescence data indicated that EGFP-*OsPIP1;3* was typically localized at the plasma membrane in mammalian cells, whereas EGFP was found throughout the cells (Figure S4a,b). Western blotting data indicated that both EGFP and EGFP-*OsPIP1;3* fusion protein was properly expressed within the cells by using anti-GFP antibody (Figure S4c). When the cells expressing EGFP-*OsPIP1;3* were exposed to 0 or 150 mM NO_3^- solution, the electrode voltage–current curves increasingly diverged from each other (upper right panel in Figure 4a), whereas little divergence occurred in the cells expressing EGFP exposed to 0 or 150 mM NO_3^- solution (upper left panel in Figure 4a). Surprisingly, the expression of *OsPIP1;3* did not lead to significant divergence of the electrode voltage–current curves in 0 or

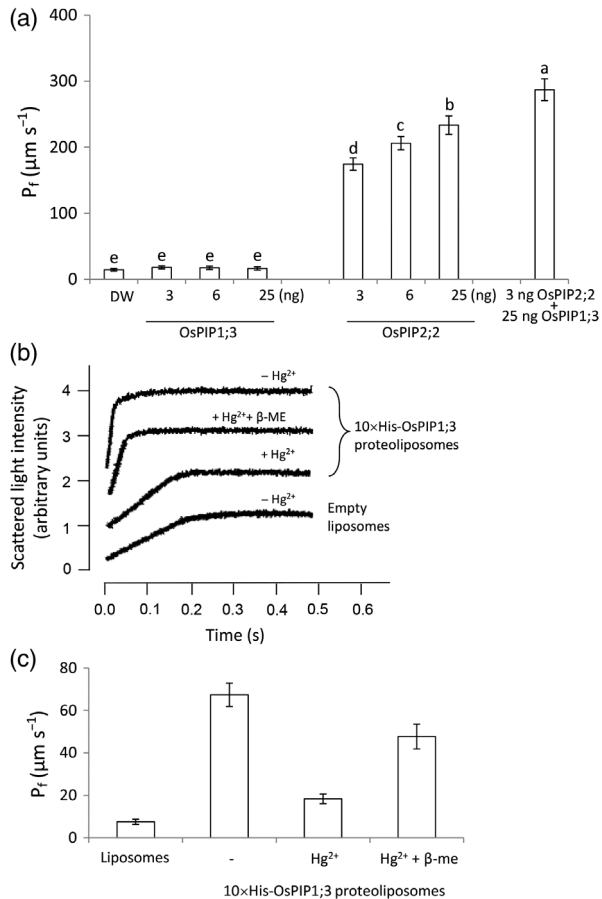


Figure 3. Functional characterization of water channel activity of OsPIP1;3. (a) Measurement of water permeability of OsPIP1;3 in the *Xenopus* oocyte system. The coefficient of osmotic water permeability (y-axis) is expressed as $P_f = \mu\text{m sec}^{-1}$. Vertical bars represent means of 10 replications \pm SEs and the different lowercase letters were significantly different (Duncan's multiple range test: $P < 0.05$). (b) The traces of stopped-flow light-scattering data. Purified 10xHis-OsPIP1;3 protein was functionally reconstituted into liposomes to obtain proteoliposomes. A portion of proteoliposomes was incubated with 300 μM of the AQP blocker HgCl_2 (+Hg²⁺) for 5 min, and a portion of Hg²⁺-treated proteoliposomes was incubated with 10 mM β -mercaptoethanol (+Hg²⁺+β-ME) for 15 min. The water permeability of proteoliposomes or empty liposomes with or without the above treatments were measured by stopped-flow light scattering; (c) Statistical analyses of P_f values of the coefficient of osmotic water permeabilities. All P_f values are expressed as means \pm SEs ($n = 10$).

150 mM $\text{HCO}_3^-/\text{CO}_3^{2-}$ solutions (lower panels in Figure 4a). The statistical data indicated that OsPIP1;3 has significant NO_3^- permeability but not $\text{HCO}_3^-/\text{CO}_3^{2-}$ exchange activity (Figure 4b), implying that OsPIP1;3 can specifically transport the NO_3^- anion across membranes besides water in mammalian cells.

Enhancement of plant growth by expressing OsPIP1;3

To investigate the physiological functions of OsPIP1;3 *in planta*, we inserted the *OsPIP1;3* gene into a binary vector (Figure S5a) in order to ectopically overexpress it in tobacco. Expression levels of endogenous *NtAQP1* and

overexpressed *OsPIP1;3* genes were detected by qPCR from the wild type and four representative T₂ progeny. The endogenous *NtAQP1* gene had similar background expressions in both wild-type and transgenic tobacco lines but *OsPIP1;3* was only expressed in the transgenic plants (Figure S5b). The *OsPIP1;3* protein expression levels in homozygous T₂ lines transformed with *FLAG-OsPIP1;3* or the empty vector were detected by anti-FLAG antibody (Figure 5a). All transgenic and wild-type plants were grown under the same conditions. The plant growth rates (plant heights) were monitored at every point in the interval and the results showed that the transgenic plants grew faster with greater height and thicker canopy than the wild-type plants at approximately 1 month after germination (Figure 5c). Figure 5(b) shows the different growth vigor of 2-month-old wild-type and transgenic plants that were re-watered and recovered from a 6-day drought treatment (Figure 6a). Moreover, the transgenic plants had greater biomass accumulation with greater fresh and dry weights than the wild type (WT) (Figure 5d).

To decipher the mechanisms of how OsPIP1;3 promoted plant growth, we determined and compared the photosynthetic physiological indexes of young WT and *OsPIP1;3* transgenic tobacco plants of the same age. We measured and calculated the leaf photosynthesis rate (A_N), transpiration rate (T_r), stomatal conductance (g_s), intercellular CO₂ concentration (C_i), leaf mesophyll conductance to CO₂ (g_m) and chloroplast CO₂ concentration (C_c). The resulting data indicate that the transgenic plants had higher A_N , g_m and C_c values than the WT plants (Figure 5e–g), whereas their g_s , T_r and C_i values were similar (Figures S6–S8), suggesting that OsPIP1;3 as well as *NtAQP1* (Uehlein *et al.*, 2003; Flexas *et al.*, 2006) promoted leaf mesophyll conductance of CO₂ gas and could enhance photosynthesis efficiency. In addition, the total chlorophyll and nitrogen contents were measured and compared between OsPIP1;3 transgenic and WT leaves. Although OsPIP1;3 demonstrated *in vitro* nitrate permeability in this work (Figure 4), the average chlorophyll and total nitrogen contents in transgenic and WT plants did not significantly differ (Figure S9a,b).

To further confirm the CO₂ permeability of OsPIP1;3, FLAG-tagged OsPIP1;3 was heterogeneously expressed in *Synechococcus elongatus* PCC 7942 cyanobacterial cells according to our protocol (Ding *et al.*, 2013). Western blot indicated that OsPIP1;3 was properly expressed in cyanobacterium (Figure S10a). On solid medium, although the transgenic and the WT cell lines looked similarly weak in CO₂-free air, they began to differ in normal air, where the transgenic line grew stronger than the WT, indicating that OsPIP1;3 may mediate CO₂ permeability across thylakoid membranes to enhance cyanobacterial photosynthesis and growth (Figure S10b). In liquid medium, the transgenic and the WT lines were cultured with equal

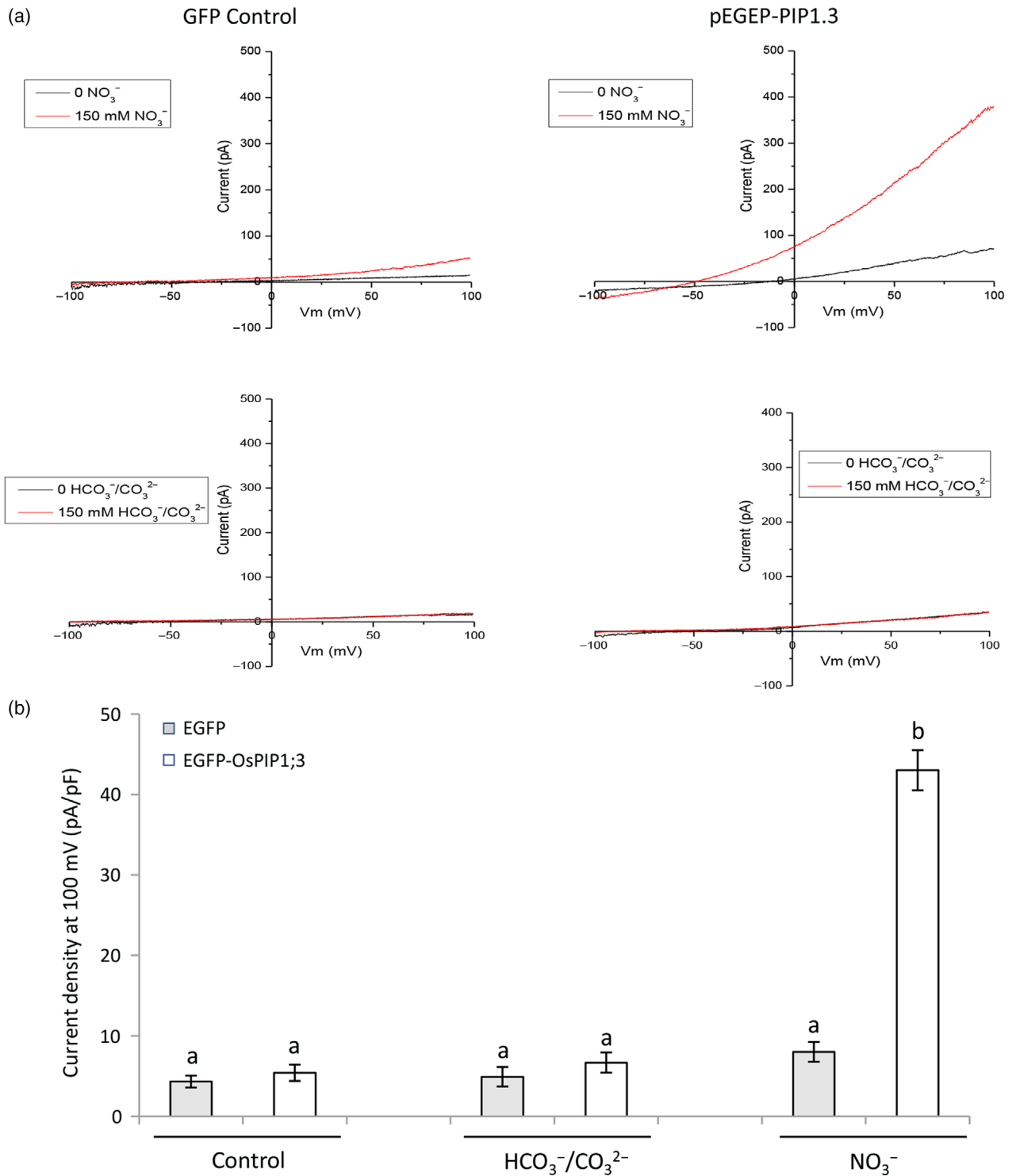


Figure 4. Measurement of nitrate permeability of *OsPIP1;3* by patch-clamp technique. (a) EGFP or EGFP-*OsPIP1;3* was expressed in mammalian HEK293 cells. At 48 h after transformation, the cells were trypsinized and exposed to $\text{HCO}_3^-/\text{CO}_3^{2-}$, NO_3^- or the control solution. The electrode voltage-current curves were detected by patch-clamp technique. (b) Statistical analyses of relative nitrate permeability. All electrophysiological recordings were repeated at least five times using different patches. Bars with different lowercase letters were significantly different (Duncan's multiple range test: $P < 0.05$).

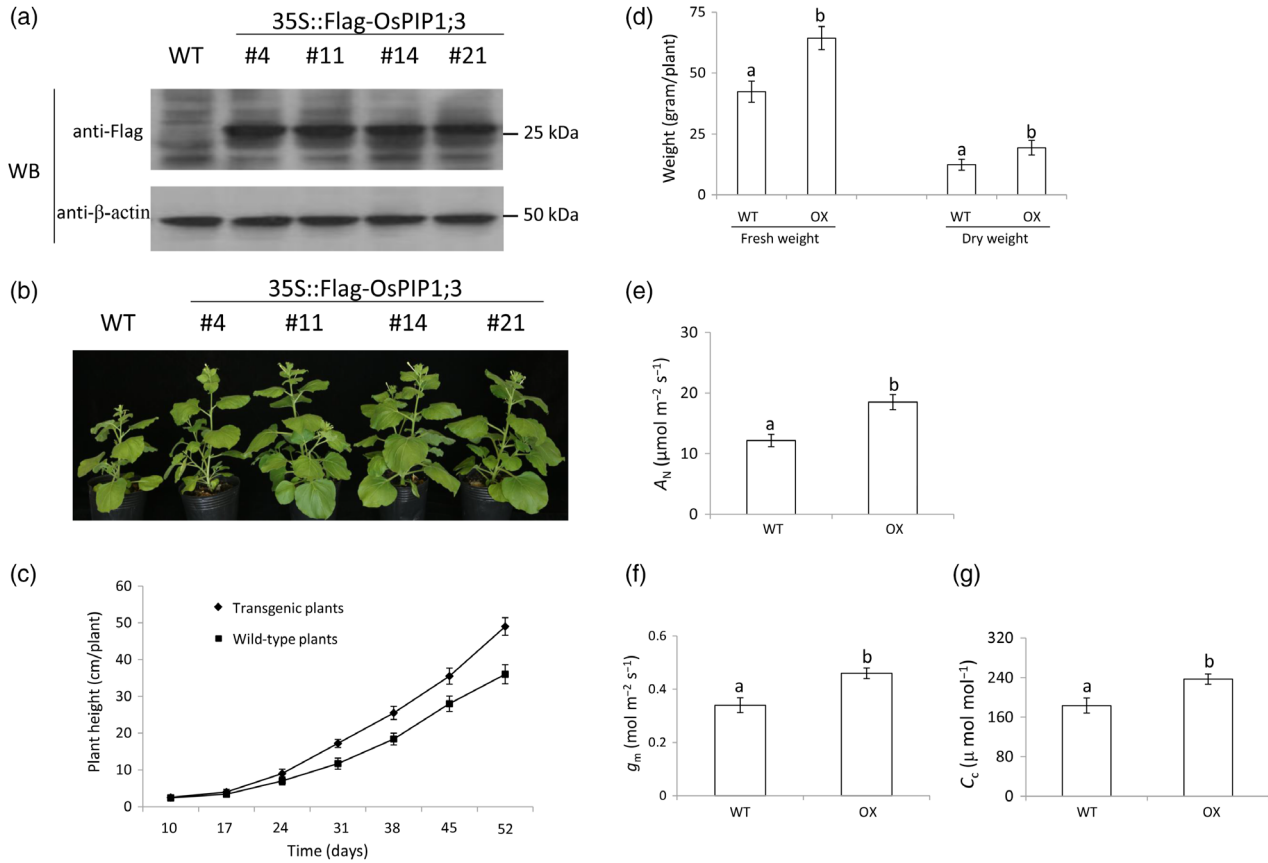


Figure 5. Growth patterns and physiological indexes of the transgenic and wild-type (WT) *Nicotiana benthamiana* (tobacco) plants. (a) Western blotting of Flag-OsPIP1;3 from the transgenic and WT tobacco lines. (b) Phenotypes of 50-day-old transgenic and WT plants. (c) Plant growth rates. (d) Fresh and dry weights per plant at 2 months old. (e) Photosynthesis rates (A_N). (f) Leaf mesophyll CO_2 conductance (g_m). (g) Chloroplast CO_2 concentration (C_c). Bars with different lowercase letters were significantly different (Duncan's multiple range test: $P < 0.05$).

initial cell densities, but the transgenic line demonstrated faster growth than the WT line in the exponential growth phases (Figure S10c).

Promotion of water transport *in planta* by OsPIP1;3 expression

To assess the effect of OsPIP1;3 overexpression on plant tolerance to water deficit, we withheld water from 2-month-old tobacco plants growing in pot soil for a total of 6 days in a growth chamber. After the 6-day drought treatment, the soil relative water content (SRWC) in all pots dropped from 85% to approximately 40% (Figure S11). The phenotypes were observed and recorded photographically. Our observation indicated that the WT plants wilted earlier than the transgenic lines after drought treatment (Figure 6a), but that all could recover soon after being re-watered (Figure 5b). To compare the water loss rates of transgenic and WT plants, we measured the relative water content of intact leaves (RWC_i) on WT and OsPIP1;3 overexpression (OX) plants before and after the plants were given 6-day drought treatment, and also measured the

relative water content of detached leaves (RWC_d) from the WT and the OsPIP1;3 OX plants before and after the leaves were dried for 3 h at room temperature. The data indicated that the RWC_i values of transgenic lines were significantly greater than those of the WT plant after 6 days of water depletion. The RWC_d values did not differ, however (Figure 6b). Further investigation indicated that the transgenic and the WT leaves had the same stomatal densities (Figure S12), suggesting that the overexpression of OsPIP1;3 may result in greater water supply from the roots rather than differing water loss (T_r) from the leaves.

To confirm the above hypothesis, we used 1-month-old transgenic and WT tobacco plantlets to measure root hydraulic conductivity ($L_{p,r}$) in a pressure chamber (Figure S13). As a result, the $L_{p,r}$ values of transgenic and WT plants were similar when plants were grown in optimal conditions. The $L_{p,r}$ values significantly differed after the plantlets were treated with 20% PEG, however. The transgenic plants had higher root hydraulic conductivities than the WT plants under stress conditions (Figure 6c), further confirming that OsPIP1;3 may function as an active water

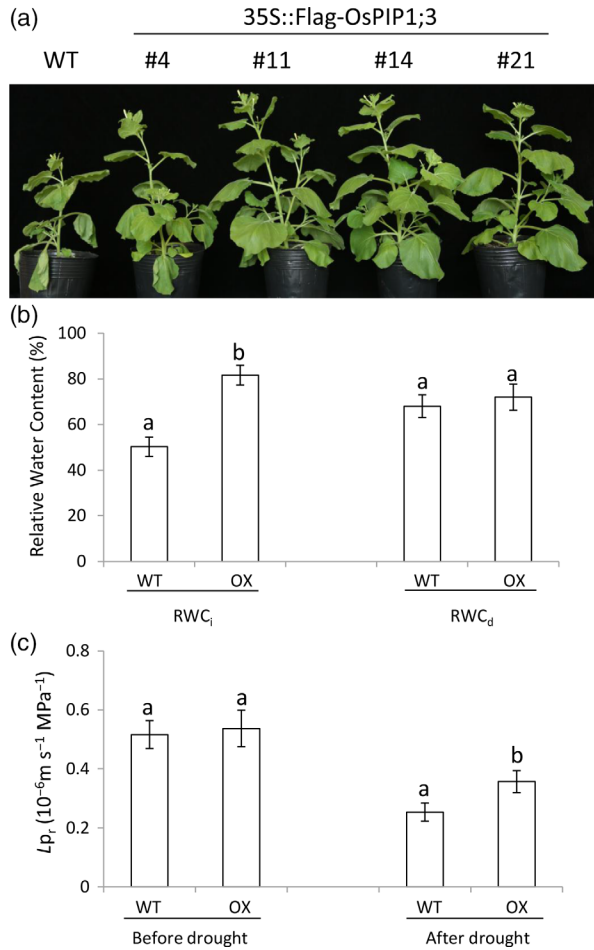


Figure 6. Analyses of water-deficit resistance and root hydraulic conductivity.

(a) The phenotypes of plants after water withdrawal for 6 days. (b) Relative water contents (RWCs) in leaves. The fresh leaves on transgenic and wild-type (WT) plants subjected to a 6-day drought treatment were picked and weighed, and their dry weights were measured after dehydration at 85°C for 1 h. The relative water contents of intact leaves (RWC_i) or detached leaves (RWC_d) were calculated. (c) Root hydraulic conductivities ($L_{p,r}$) before and after 20% PEG treatment. Bars with different lowercase letters were significantly different (Duncan's multiple range test; $P < 0.05$).

channel *in planta* to enhance water uptake from the soil and thereby promote plant resistance to water deficit.

Enhancement of water-use efficiency (WUE) by *OsPIP1;3* expression

As the transgenic plants showed more vigorous growth than the WT plants, this led us to investigating how *OsPIP1;3* expression affects WUE. To this end, we grew 1-month-old WT and OX plantlets under well-irrigated conditions with the relative soil water content (RSWC) held at 85%. The pots were covered with a gas-resistant foil to minimize evaporation. Growth was assessed by monitoring leaf area, leaf number and plant height over time. Each

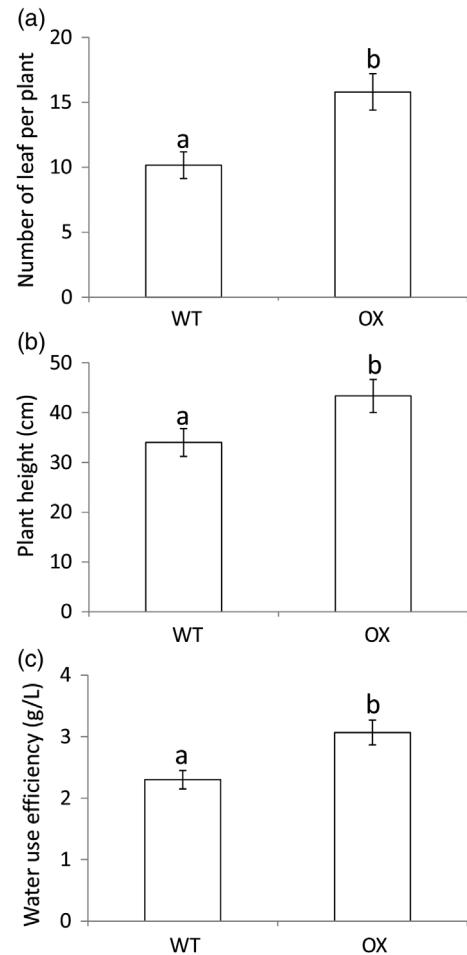


Figure 7. Overexpression of *OsPIP1;3* increased the water-use efficiency (WUE) of *Nicotiana benthamiana* (tobacco) plants.

One-month-old transgenic and wild-type (WT) tobacco plantlets were grown in pot soils with 85% relative water content. The pots were covered with foil to prevent water evaporation and were irrigated every 4 days for a total of 32 days. (a) Average numbers of expended leaves. (b) Average plant height. (c) Water-use efficiency (WUE). Bars with different lowercase letters were significantly different (Duncan's multiple range test; $P < 0.05$).

pot was irrigated with an equal volume of water every 4 days. After 32 days, the leaf area, leaf number and plant height were measured and each individual plant was harvested and weighed. The data show that the transgenic plants had greater leaf number, plant height and WUE values than the WT plants (Figure 7a–c), but that leaf area did not differ (Figure S14).

DISCUSSION

Plants are sessile and cannot escape from their surroundings. Thus, they must adapt to varying environmental conditions through various molecular responses. Water is one of the most important molecules for all living organisms. The regulation of water transport is crucial for many physiological activities, e.g. absorption, transpiration and

respiration. Most AQPs are tetrameric channel proteins allowing the transmembrane passage of small solutes and water into and out of living cells (Gena *et al.*, 2011). In plants, members of the PIP AQP subfamily are important for the maintenance of plant water status through the control of cell and tissue hydraulics. We identified the SNPs of *OsPIP1;3* genes from two rice subspecies. In sorghum, hundreds of SNPs were identified from AQP loci among 50 sorghum accessions and most of the SNPs are related to the expression of AQP genes in response to waterlogging stress (Kadam *et al.*, 2017).

Like other plant PIP1s, single *OsPIP1;3* showed abnormal cellular localization and negligible water channel activity. Most PIP1 channels fail to be targeted to the plasma membrane and reside in intracellular membranes, typically the ER when heterologously expressed in oocytes or yeast, or even in plant cells (Katsuhara *et al.*, 2002; Liu *et al.*, 2013). The intracellular retention of PIP1s is either caused by missing plasma membrane trafficking signals or by existing ER retention motifs, whereas the interaction and heterotetramerization of certain pairs of PIP1s and PIP2s can significantly enhance water permeability (Bienert *et al.*, 2018). For example, the combinations of *OsPIP1;1/OsPIP2;1* (Liu *et al.*, 2013), *OsPIP1;3/OsPIP2;2* (this work) and *BvPIP1;1/BvPIP2;1* (Jozefkiewicz *et al.*, 2013) could significantly enhance PIP1 activities through their physical interactions with PIP2s. The influence of AQPs on hydraulic conductance in plants is important in regulating the plant transpiration rate, particularly under conditions of developing soil water deficit stress and elevated atmospheric vapor pressure. As AQPs represent a big gene family, only some members are involved in the response to water deficit and drought stress (Lian *et al.*, 2006; Song *et al.*, 2018). Genetic engineering has brought insights to the physiological functions of AQPs, and has increased our understanding of their roles in water transport and abiotic stress responses. In *Arabidopsis*, the expression of *AtPIP1;3*, *AtPIP1;4*, *AtPIP2;1* and *AtPIP2;5* increased but the expression of *AtPIP1;5*, *AtPIP2;2*, *AtPIP2;3* and *AtPIP2;6* decreased in response to drought stress (Jang *et al.*, 2004). Alexandersson *et al.* (2005) reported that the expression of *AtPIP1;3* and *AtPIP2;1* decreased in response to drought stress, however. In this work we demonstrated that the expression of *OsPIP1;3* could be transcriptionally and translationally induced by drought stimulus (Figure 1b,c). *OsPIP1;3* showed various response patterns to drought in upland and lowland rice cultivars (Lian *et al.*, 2006), however, indicating that PIP expression induced by water deficit is a complicated response and that the molecular mechanisms underlying the regulation of PIP expression in drought conditions remain elusive. Here, we revealed experimentally that the overexpression of *OsPIP1;3* enhanced root hydraulic conductance and WUE in transgenic tobacco plants compared with WT plants. Plant

WUE, represented by the ratio of carbon assimilation to water consumption, describes the efficiency of a plant in optimizing carbon gain while minimizing water loss. In practical terms, high WUE is important for agriculture in water-deficient areas and improved WUE confers a competitive advantage when water is limited. Intriguingly, AQPs have been proven to be the major determinants of WUE in plants (Flexas *et al.*, 2013a). Constitutive overexpression of the fungal *ThAQGP* gene enhanced the photosynthetic rate of tobacco plants under water stress and hence increased the efficiency of water use, despite the high transpiration rate. The conservation of the higher transpiration rate is an interesting mechanism that ensures not only continuous CO₂ uptake but also the continued supply of nutrients, reduced leaf temperature and enhanced plant growth (Vieira *et al.*, 2017).

We previously found that *OsPIP1;3* might play an important role in rice drought avoidance by the rapid rolling of leaves to minimize water transpiration (Lian *et al.*, 2004). The conversion from drought avoidance to drought resistance is probably achieved through enhanced root hydraulic conductivity, ensuring water supply but not reducing water evaporation in *OsPIP1;3* transgenic tobacco plants. It has been reported that AQPs contribute up to 80–90% of rice root hydraulic conductivity (*L_p*) under well-watered and drought conditions, and that root plasma membrane aquaporin (PIP) expression and root anatomical properties correlate with hydraulic traits (Grondin *et al.*, 2016). Matsuo *et al.* (2009) reported that different genotypic and ecotypic rice cultivars demonstrated different root hydraulic conductivities under hydroponic or aerobic water regimes. In flooding conditions, the root hydraulic conductance of most rice cultivars were greatly restrained and showed similar effects on shoot growth; however, in water-saving or drought conditions, different genotypic cultivars demonstrated various root hydraulic conductances, directly resulting in differing resistance to water deficiency. The *OsPIP1;3* gene in an upland rice cultivar (subspecies *indica* cv. Zhonghan 3) was responsive to drought stress and overexpression of *OsPIP1;3* in stress-sensitive lowland rice (subspecies *japonica* cv. Zhonghua 11) improved its water status by increasing root conductivity (Lian *et al.*, 2004), thereby confirming our observations in tobacco.

Ectopic expression of plant AQP genes like *Musa* (banana) *MaTIP1;2*, apple *MdPIP1;3* and *Arabidopsis PIP1b* enhanced plant resistance to water deficit under osmotic stress or extreme temperatures (Almeida-Rodriguez *et al.*, 2010; Wang *et al.*, 2017a; Song *et al.*, 2018). Apple *MdPIP1;3* allowed for more rapid guard cell engorgement in transgenic leaves and therefore resulted in reduced water loss through stomata under drought conditions (Wang *et al.*, 2017a). Interestingly, the overexpression of an aquaglyceroporin, *ThAQGP*, from the fungus *Trichoderma harzianum* could also show active channel functions

and conferred significant drought resistance in tobacco by presenting a higher transpiration rate, stomatal conductance, photosynthetic efficiency and WUE than found in the wild-type specimen (Vieira *et al.*, 2017). Some other AQPs conferred decreased stress tolerance, however (Aharon *et al.*, 2003; Wang *et al.*, 2015).

It has been suggested that drought stress tolerance in aquaporin-overexpressing plants is closely related to aquaporin water transport activity in the roots, increasing the ability to retain water (Zhuo *et al.*, 2016). Almost all *OsPIP1;3* transgenic lines had higher fresh shoot and root weights than the WT under stress conditions, suggesting that plants adjust water content by modifying their ability to retain water in shoots and roots. Functional analyses using aquaporins predict their roles in plant–water relationships. When the aquaporin gene is silenced in a plant, decreased cellular osmotic water permeability and reduced water stress resistance are observed (Kaldenhoff *et al.*, 1998).

The timely closure of stomata in water-deficit conditions is a complicated physiological process. It has been reported that some AQPs directly participate in stomatal closure. Arabidopsis *AtPIP2;1* is phosphorylated and activated by OST1 (SnRK2.6) in guard cells to facilitate water and H₂O₂ flux and stomatal closure (Rodrigues *et al.*, 2017). The *in planta* and *in vitro* data from our study show that *OsPIP1;3* can conduct water and NO₃[−] across the membrane system, although whether *OsPIP1;3* directly participates in stomatal closure or not needs to be elucidated further. The plant anion channel SLAC1 can be activated by nitrate to induce stomatal closure (Hedrich and Geiger, 2017); however, the sensitivity of monocot and dicot SLAC1s to nitrate-dependent stimulus differs fundamentally. Further evidence shows that when the motif of nitrate-insensitive *AtSLAC1* was replaced by a tandem amino acid residue motif in the *HvSLAC1* anion channel of guard cells in *Hordeum vulgare* (barley), *AtSLAC1* was converted into a grass-type nitrate-sensitive channel (Schäfer *et al.*, 2018), indicating that nitrate is an important signaling molecule in plant stomatal closure. Hence, we can postulate that the enhancement of nitrate uptake from soil and transport in *OsPIP1;3* transgenic plants may be one of the triggers for guard cell closure through activating anion channels like SLAC1 and SLAH3 under water-limiting conditions, although this hypothesis must be confirmed experimentally.

Plant SnRK2 kinase OST1 is a major kinase in regulating stomatal closure through phosphorylating anion channels. SnRK1s have many functions that are broadly and synergistically involved in the metabolism of nitrogen/carbon and in responses to biotic/abiotic stress (Crozet *et al.*, 2014). In our recent work, we identified that a PIP1 of wild soybean interacts with SnRK1 kinase, and found that its S131 residue in the first inner loop of GsPIP1 was a

potential phosphorylation site of SnRK1 (Song *et al.*, 2019). This putative phosphorylation site is highly conserved in all PIP1 homologs. Like OST1 phosphorylating S121 to determine the activity of *AtPIP2.1*, SnRK1 may affect its substrate permeability by phosphorylating the S131 residue. For example, rice plasma membrane receptor-like kinase leaf panicle 2 (LP2) physically interacted with *OsPIP1;1*, *OsPIP1;3* and *OsPIP2;3* in the plasma membrane. Intriguingly, it negatively affected drought resistance by promoting stomatal opening and decreasing the H₂O₂ level in the guard cells (Wu *et al.*, 2015), suggesting that the expression of PIPs including *OsPIP1;3* may be generally altered by the upstream signals to actively participate in the maintenance of water homeostasis in plants.

In our work, the *OsPIP1;3* transgenic plants grew more vigorously than the WT plants. *OsPIP1;3* might enhance the uptake of carbon and nitrogen, and subsequently promoted plant photosynthesis and growth. Previous reports indicated that some AQPs could enhance leaf mesophyll CO₂ conductance (g_m), photosynthesis (A_N) and hydraulic conductivity (Nakhoul *et al.*, 1998; review by Flexas *et al.*, 2006; Groszmann *et al.*, 2017). The conductance of CO₂ in photosynthesizing leaves is commonly divided into three components: boundary layer, stomatal, and mesophyll conductance. Mesophyll conductance (g_m) is the most restricted sense of a physical diffusion phenomenon. Any of these components, but especially mesophyll conductance with low diffusion, poses a limitation to photosynthesis whenever CO₂ levels are not saturated. Similar to our work, when the *OsPIP1;2* gene from *Oryza sativa* L. cv Nipponbare was overexpressed in rice, the transgenic rice lines had significantly higher photosynthesis rate and biomass accumulation (Xu *et al.*, 2019). Overexpression of the *NtAQP1* gene in tobacco increased g_m and the net photosynthesis rate, measured using a combination of gas exchange, chlorophyll fluorescence and on-line ¹³C isotope discrimination techniques. It was reported that Arabidopsis had an unexpected lower g_m than was reported for other annual plants, and the low g_m and low capacity for carboxylation were major factors in limiting photosynthesis (A_N) (Flexas *et al.*, 2007).

Here, we observed that ectopic expression of *OsPIP1;3* in tobacco and heterogeneous expression of *OsPIP1;3* in cyanobacteria did promote photosynthesis and growth of the transgenic plants and cyanobacteria. Nevertheless, our previous work indicates that cyanobacterium *Synechococcus* sp. PCC7942 has only one aquaporin-like gene, and that knock-out of this gene caused significant abrogation of CO₂ uptake and the inhibition of cell growth (Ding *et al.*, 2013). Plant AQPs like tobacco *NtAQP1* (Uehlein *et al.*, 2003), *AtPIP2;1* (Wang *et al.*, 2016) and *HvPIP2s* (Mori *et al.*, 2014) were reported to mediate CO₂ permeability across the membranes, and to promote photosynthesis and plant growth. By mutagenesis, Mori *et al.* (2014) reported that

I254 of HvPIP2;3 was a key residue in the sixth TM domain to determine its CO₂ permeability, and the substitution of isoleucine with methionine (I245M) abolished CO₂ permeability in HvPIP2;4. By sequence alignment, OsPIP1;3 also has an isoleucine residue in the corresponding site (Figure S1), suggesting that OsPIP1;3 may possess CO₂ permeability, and supporting our observation that OsPIP1;3 overexpression plants grew better and accumulated more biomass than the WT plants. Because CO₂ and water vapor share a common diffusion pathway from the air to the spaces inside leaves, an analysis of water vapor fluxes allows for accurate estimates of boundary layer and stomatal diffusion conductance. Plant WUE, represented by the ratio between carbon gain (photosynthesis) and water loss (transpiration), describes the efficiency of the plant in optimizing carbon gain while minimizing water loss. Improved WUE confers a competitive advantage when water is limited, and aquaporins are major determinants of WUE in plants (Flexas *et al.*, 2013a). The importance of mesophyll conductance (g_m) in optimizing water use during drought is shown by the correlated changes in mesophyll conductance and WUE (Maurel *et al.*, 2016). In our work, overexpression of the *OsPIP1;3* gene in tobacco plants seems to increase leaf WUE and could be explained by gas-exchange results and water balance.

In practice, sustainable agriculture requires a major reduction in water use and in fertilizer use. It is therefore imperative to improve not only yields but also water productivity or WUE, i.e. the amount of carbon gained per unit water used, as well as nitrogen-use efficiency (NUE). Nitrate is an important nutrient mineral for plants. The uptake and transport of nitrogen nutrients are fulfilled by multiple pathways. Besides high- and low-affinity nitrate transporters like NRT2.1 and NRT2.4, some other channels may also possess these functions. In plants, the expression of MfPIP2-7 from *Medicago falcate* could enhance plant growth under NO₃⁻-deficient conditions (Zhuo *et al.*, 2016). Until now, only human AQP6 was reported to allow the transport of nitrate. The point mutation Asn60Gly converted AQP6 from an anion channel to a water channel (Ikeda *et al.*, 2002) and Leu51Arg converted AQP5 from a water channel to an anion channel, demonstrating the anion permeability sequence I⁻ > NO₃⁻ ≅ NO₂⁻ > Br⁻ > Cl⁻ > HCO₃⁻ > gluconate (Qin and Boron, 2013), suggesting that key individual residues in these channels determine their important properties. In this work, we determined the *in vitro* NO₃⁻ permeability of OsPIP1;3 by patch-clamp technique, and compared root hydraulic conductivities, growth properties and WUE between OsPIP1;3 transgenic and WT plants. The data clearly indicate that OsPIP1;3 significantly improved the related physiological indexes. In *Helianthus annuus* (sunflower), the nitrate availability greatly and rapidly affected dynamic changes in root hydraulic resistance. The sunflower roots became more

permeable to water within 20–30 min after the application of nitrate and this increase in permeability continues over time, with the maximum enhancement dependent upon the nitrate concentration (Gloser *et al.*, 2007). The experiments with *Lotus japonicus* also showed that significant changes in root hydraulic properties occurred following nitrate supply (Clarkson *et al.*, 2000). Moreover, at the transcriptional level, the array assay revealed that the expression of many AQP genes could be induced by nitrate in tomato (Wang *et al.*, 2001). Hence, NO₃⁻ is not only a nutrient for plant growth but is also a signaling molecule that affects PIP expression at both transcriptional and translational levels to govern plant root hydraulic conductivity (L_p) (Li *et al.*, 2016). Similarly, nitric oxide (NO) was also reported to be an elicitor to stimulate the transcription of OsPIP1;1, OsPIP1;2, OsPIP1;3 and OsPIP2.8 in rice germinating seeds (Liu *et al.*, 2007). In our scenario, how nitrate affects AQP functions and how AQPs affect nitrate uptake and transport *in planta* are still matters for further investigation.

Overall, we systematically characterized the water and nitrate permeability of OsPIP1;3 from a drought-resistant rice variety by biochemical and biophysical approaches. The expression of OsPIP1;3 enhanced plant drought resistance and vegetative growth, offering the opportunity to advance a more holistic understanding of the additional functions played by plant AQPs and providing insights into their translational potential.

EXPERIMENTAL PROCEDURES

Materials, gene cloning and construction of DNA plasmids

The seeds of rice *O. sativa* L. *indica* cv. Zhonghan 3 and tobacco (*N. benthamiana*) were obtained from the Key Laboratory of Agricultural Biological Functional Genes, Northeast Agricultural University, China, and the Institute of Biotechnology, Akita Prefectural University, Japan. Anti-OsPIP1;3-specific antibody (cat no. AS09 504) was purchased from Agrisera AB (<https://www.agrisera.com>). Anti-FLAG (cat no. F3165-2MG) and anti-GFP (cat no. G1546) antibodies were purchased from Sigma-Aldrich (<https://www.sigmaaldrich.com>).

The plasmids bearing the complete ORFs of *OsPIP1;3* and *OsPIP2;2* genes were isolated from a rice cDNA library. The genes flanked by *Bgl*II were inserted into the pXβG-ev1 vector to result in pXβG-OsPIP1;3 and pXβG-OsPIP2;2 for expression in *Xenopus laevis* oocytes or pXβG-OsPIP1;3-EGFP and pXβG-OsPIP2;2-EGFP for the visualization of expression of these genes in oocytes. For gene transient expression in rice protoplasts, the plant gene expression cassette (35Spro-MCS-NOS3ter) was inserted into the pUC18 vector. *OsPIP1;3-EGFP* or *OsPIP2;2-mDsRed* was cloned into *Sall* and *Eco*RI sites to generate pUC18-OsPIP1;3-green or pUC18-OsPIP2;2-red. To maximize the production of recombinant OsPIP1;3 protein in *E. coli*, the codons of the *OsPIP1;3* gene were modified by referring to preferential codons of *AqpZ* and *AqpM* (Calamita *et al.*, 1995; Kozono *et al.*, 2003). The optimized sequence was synthesized at Blue Heron (<http://www.blueheronbio.com>). The plasmid pTrc10HisAqpZ (Borgnia *et al.*, 1999) was digested with *Eco*RI and *Sall* to release *AqpZ* for insertion of *OsPIP1;3* to generate pTrc10His-OsPIP1;3 with a 10×His tag

(MGHHHHHHHHSSIEGRHEF) in the N terminus of *OsPIP1;3*. To generate the transgenic plants, the 35Spro-Flag-*OsPIP1;3*-NOS3ter cassette was inserted into *EcoRI* and *SacI* sites of the Ti plasmid binary vector pPBEL, derived from pCambia2300, to obtain pPBEL-Flag-*OsPIP1;3*.

Injection into *Xenopus* oocytes and measurement of osmotic water permeability

The general procedure was similar to a previously described protocol (Liu *et al.*, 2013), with some modifications. Briefly, the capped complementary RNA (cRNA) samples were synthesized using T₃ RNA polymerase of the mMESSAG mMACHINE High Yield Capped RNA Transcription Kit (Ambion, now ThermoFisher Scientific, <https://www.thermofisher.com>) after linearization of the pXβG-*OsPIP1;3* plasmid. Fresh oocytes (1.0–1.2 mm in diameter) of stage V–VI were treated with 0.1% collagenase (*Clostridium histolyticum*, type II; Sigma-Aldrich) to exfoliate the oocyte membrane. A 50-nl (10–50 ng) volume of cRNA solution or water was injected into the oocytes using a nanoject injector (Narishige, <http://narishige-group.com>). The injected oocytes were incubated in 2-(*N*-morpholine)-ethanesulphonic acid (MES)-buffered saline (MBS; 200 mOsm_{in}) for 48 h at 20°C. The fluorescence generated by the chimeric *OsPIP1;3*-EGFP protein could be observed under a confocal laser scanning microscope. To measure water channel activity, the injected oocytes were transferred into hypotonic solution (one-third diluted MBS, 70 mOsm_{out}). The sizes of the oocytes at intervals of 1 sec were captured by digital camera (Shimadzu, <https://www.shimadzu.com>), and the swelling rates of oocytes at each time point were calculated with MOTIC IMAGES PLUS 21s (Shimadzu). Water permeability (coefficient of osmotic water permeability, P_f) was calculated as previously described (Kozono *et al.*, 2003).

Expression and purification of recombinant *OsPIP1;3*

The pTrc10His-*OsPIP1;3* construct obtained was transformed into *E. coli* strain BL21-CodonPlus(DE3)-RIL (Stratagene, now Agilent, <https://www.agilent.com>). The cells were grown in 10-L Luria Bertani (LB) medium in a fermentation tank to an OD₆₀₀ of 1.5 prior to the addition of isopropyl-β-D-thiogalactoside at a final concentration of 1 mM, and then vigorously shaken at 37°C for 2 h. The cells were harvested and resuspended in 120 ml of ice-cold lysis buffer (100 mM K₂HPO₄, 1 mM MgSO₄, 0.4 mg ml⁻¹ lysozyme, 0.1 mg ml⁻¹ DNase I, and 1 mM phenylmethylsulfonyl fluoride) and then subjected to three French press cycles (1266 kg cm⁻²) at 4°C. The cell lysates were centrifuged at 6000 g for 10 min at 4°C. The supernatants were transferred to fresh tubes and were ultracentrifuged at 200 000 g for 60 min at 4°C. To efficiently extract 10×His-*OsPIP1;3* protein, the membrane pellets were incubated with solubilization buffer (25 mM Na₂HPO₄, 10% (v/v) glycerol, 5 mM β-mercaptoethanol, and 125 mM NaCl, pH 8.0) containing 5% or 10% OG (*n*-octyl-β-D-glucoside), 5% DM (*n*-dodecyl-β-D-maltoside), 5% C12E8 (octaethylene glycol monododecyl ether), 5% OPOE (*n*-octylpolyoxyethylene), 3% LDAO (*N,N*-dimethyldodecylamine *N*-oxide), 1.5% FC12 (Fos-choline 12) and 0.4% or 4% PFO (perfluorooctanoic acid), with gentle agitation at 4°C overnight. All of the samples were centrifuged at 100 000 g for 60 min at 4°C to pellet the insoluble materials. Equal volumes of the supernatant were resolved in 12% SDS-PAGE gels. The protein extraction efficiency using different detergents could be evaluated by Western blotting using anti-*OsPIP1;3* antibody. The purification of recombinant 10×His-*OsPIP1;3* was performed by mixing with prewashed Ni-NTA agarose beads and incubated with gentle agitation at 4°C overnight. The beads were washed with cold wash buffer (2% detergent, 100 mM K₂HPO₄, 10% glycerol, 5 mM β-

mercaptoethanol, 200 mM NaCl, and 100 mM imidazole, pH 7.0) three times to remove nonspecifically bound materials. Recombinant 10×His-*OsPIP1;3* was eluted with 2 ml of elution buffer (0.4% PFO, 25 mM Na₂HPO₄, 10% glycerol, 5 mM β-mercaptoethanol, 150 mM NaCl, and 1 M imidazole, pH 7.0). The protein obtained was subsequently dialyzed and concentrated for functional characterization.

Liposomal reconstitution and functional characterization of 10×His-*OsPIP1;3*

The purified 10×His-*OsPIP1;3* protein produced from above was reconstituted into liposomes as previously described (Borgnia *et al.*, 1999). Briefly, reconstitution mixtures were prepared at 23–28°C room temperature by the sequential addition of the following solutions to certain concentrations: 100 mM 3-(*N*-morpholino) propanesulfonic acid (MOPS; pH 7.5), 1 mM NaN₃, 1 mM dithiothreitol (DTT), 1.25% (w/v) *N*-octyl-β-D-glucopyranoside, 100 μg ml⁻¹ purified 10×His-*OsPIP1;3* protein and 9 mg ml⁻¹ of bath-sonicated *E. coli* polar lipids (Avanti Polar Lipids Inc., <https://avantilipids.com>). The mixture was vigorously vortexed and then incubated on ice for 20 min. The reconstitution mixture was rapidly passed through a 23-gauge needle into 25 volumes of reconstitution buffer [50 mM MOPS, 150 mM *N*-methyl-D-glucamine, 1 mM DTT, and 0.5 mM phenylmethylsulfonyl fluoride (PMSF)] to dilute the detergent. Proteoliposomes or liposomes were collected by centrifugation at 123 000 g, held at 4°C for 1 h, and washed three times. The lipid pellets were resuspended in reconstitution buffer. The diameters of proteoliposomes and liposomes were determined by electron microscopy.

To assess the osmotic water permeability of the 10×His-*OsPIP1;3* reconstituted proteoliposomes, light-scattering experiments were performed in a stopped-flow light-scattering apparatus, as previously described (Calamita *et al.*, 2006). The coefficient of osmotic water permeability (P_f) of the liposome or proteoliposome membranes was calculated from the K_i , as previously described (van Heeswijk and van Os, 1986), using the equation: $P_f = (K_i \cdot V_0) / (A_v \cdot V_w \cdot \Delta C)$, where K_i is the fitted exponential rate constant, V_0 is the initial mean vesicle volume, A_v is the mean vesicle surface, V_w is the partial molar volume of water (18 cm³ mol⁻¹) and ΔC is the osmotic gradient. The P_f unit is expressed as [μm³ (H₂O)]/[μm² (membrane area) × s (time)] = μm sec⁻¹. The medium osmolarity was verified by a vapor-pressure osmometer (Wescor, <http://water.wescor.com>). In some experiments, the liposome specimens were pre-incubated for 5 min with 300 mM HgCl₂, a sulfhydryl compound blocking the AQP channels. In other experiments, to verify the blocking action of the Hg²⁺ ion, the HgCl₂ treatment was followed by a 15-min exposure to 10 mM of the reducing agent β-mercaptoethanol (β-ME).

Measurement of nitrate conductance of *OsPIP1;3*

The *OsPIP1;3* gene was cloned into the pEGFP-C1 vector. The resulting construct or empty pEGFP-C1 vector was transfected into HEK293 cells grown in a six-well tissue culture dish using Lipofectamine 2000 (Life Technologies, now ThermoFisher Scientific, <https://www.thermofisher.com>). Forty-eight hours after transfection, the cells were dissociated by trypsin treatment and kept in complete serum-containing medium and were re-plated on 35-mm tissue culture dishes in a tissue culture incubator until recording. The patch-clamp assay was performed according to the method described by Hamill *et al.* (1981). The standard bath solution contained (in mM): 145 sodium methanesulfonate (Na-MS), 5 NaCl and 10 HEPES, pH 7.4. NaMS and NaCl were replaced by 150 mM NaHCO₃ or 150 mM NaNO₃ to measure HCO₃⁻ and NO₃⁻ currents,

respectively. The pipette solution contained (in mM): 145 Cs-MS, 2.5 MgCl₂, 1 EGTA, and 10 HEPES, pH 7.4. The patch pipettes were pulled from borosilicate glass (Harvard Apparatus, <https://www.harvardapparatus.com>) and heat polished to a resistance of 5–7 MΩ. Data were acquired using an AxoPatch 200B amplifier (Molecular Devices, <https://www.moleculardevices.com>) and a low-pass analogue filter set to 1 kHz. The current signal was sampled at a rate of 20 kHz using a 1322A digitizer (Molecular Devices) and further analyzed with pCLAMP 9 software (Molecular Devices). After the patch pipette was attached to the cell membrane, the giga seal (5–10 GΩ) was formed by gentle suction. The whole-cell configuration was formed by a short electric zap or suction to rupture the membrane patch. The holding potential was set to –100 mV. To obtain the current–voltage relationship curve, the membrane was ramped from the holding potential (–100 mV) to 100 mV for 1 sec and then returned to the holding potential (She *et al.*, 2018). All electrophysiological recordings were repeated at least five times using different patches. Most data points shown are means ± SEMs ($n = 5$ independent experiments).

Expression of EGFP-OsPIP1;3 in rice protoplast

The rice O.c. cell line was isolated from seedling roots of the indica-type rice *O. sativa* L. accession C5924 (Baba *et al.*, 1986) and was obtained from Dr Isao Shimamoto. The cells were subcultured at 25 ± 2°C in the dark at 2 g in Murashige and Skoog medium supplemented with 1.0 mg L⁻¹ of 2,4-dichlorophenoxyacetic acid at regular intervals of 2 weeks. The cells were harvested and treated in 4% (w/v) cellulase and 1% (w/v) Macerozyme solution at 30°C for 5 h. Afterwards, the digested cells were filtered through a steel mesh (38 μm) and the protoplasts were collected by centrifugation at 100 g for 10 min. The transient transformation of rice O.c. protoplasts was performed according to the method described by Shen *et al.* (2014). Briefly, the rice protoplasts obtained were resuspended in W5 solution (154 mM NaCl, 125 mM CaCl₂, 5 mM KCl, 2 mM MES, pH 5.8) at the desired cell density of 1.5–2.5 × 10⁶ protoplasts ml⁻¹, determined by counting the cells with a hemacytometer. Ten-forty μg of pUC18-OsPIP1;3-green or/and pUC18-OsPIP2;2-red plasmids were added to 200 μl of suspended protoplasts and gently mixed in a 2-ml centrifuge tube, and then 250 μl of PEG solution [40% (w/v) PEG 4000, 0.3 M mannitol, 0.1 M CaCl₂] was added and gently mixed. The protoplast/DNA mixture was incubated at room temperature for 20 min and was diluted with 2 ml of R2S medium, and was gently mixed by inverting the tubes to stop the transfection process. The protoplast suspension was transferred to a 35 mm × 10 mm Petri dish and was incubated for 6–18 h at 27°C. The fluorescent signals of transformed protoplasts were observed under a confocal microscope.

Endogenous OsPIP1;3 localization by immunoelectron microscopy

The rice root tips from young seedlings were fixed in 0.1 M phosphate buffer (pH 7.4) with 4% paraformaldehyde and 0.05% glutaraldehyde at 4°C for 1 h. The root samples were washed and dehydrated in 70% ethanol for 10 min and 96% ethanol for 20 min, and then were transferred into a mixture of LR-White resin (London Resin Co. Ltd, now Agar Scientific, <http://www.agarscientific.com>) and 96% ethanol (1:1) for 2 h and then in pure LR-White for 5 h. The roots were embedded in 100% LR-White gelatin capsule at 50°C for 24 h. Ultra-thin sections were cut with a diamond knife (Jumdi; Electron Microscopy Sciences, Hatfield, PA, USA, <https://www.emsdiasum.com/microscopy/default.aspx>) and then mounted on 200 nickel mesh grids. The sections were blocked in 5% BSA solution (in PBS, pH 7.2) for 2 h, and then were

immunostained with an anti-OsPIP1;3-specific rabbit antibody or rabbit serum, and were subsequently stained with gold colloid labeled anti-rabbit IgG antibody. Lastly, the ultra-thin sections were stained with TI blue and were observed with a JEM-1230 microscope (JEOL, <https://www.jeol.co.jp>).

Generation of transgenic tobacco plants

pPBEL-OsPIP1;3 plasmid harboring *OsPIP1;3* under the control of the 35S promoter and the nopaline synthase terminator was introduced into *Agrobacterium tumefaciens* EHA101 by electroporation. Tobacco transformation was performed according to the protocol previously described by Ding *et al.* (2004). Briefly, the leaves from 3-week-old tobacco plantlets growing on sterile medium were excised and cut into small pieces of approximately 0.5 cm². The leaf explants were immersed in the agrobacterial suspension for 1 min and were then transferred onto sterile filter paper for a few seconds prior to MS medium for 2 days in the dark. The leaf explants from the dark were transferred onto MS medium supplied with 1 mg L⁻¹ BAP, 100 mg L⁻¹ kanamycin sulfate and 200 mg L⁻¹ cefotaxime, and were cultured under light for 3–4 weeks. The shoots with 1 cm of height were excised from the calli and were transferred onto rooting medium. The plantlets with roots were transferred to soil in the glasshouse for propagation to generate T₂ progeny. The expression levels of OsPIP1;3 in homologous progeny were identified by qPCR and Western blotting.

Determination of root hydraulic conductivity

The hydraulic conductivities (Lp_r) of the transgenic and control roots were measured according to the method described by Murai-Hatano *et al.* (2008). Briefly, 1-month-old OsPIP1;3 and wild-type tobacco seedlings were divided into two groups. One group of plantlets were cultured in half-strength MS medium and the other group of plantlets were cultured in half-strength MS medium containing 20% PEG to mimic drought treatment for 6 h. Afterwards, individual plantlets were fixed in a pressure chamber filled with nutrient solution. In order to apply static pressure to the root medium, the gap between the stem and the metal lid was sealed with dental paste and then the upper shoot was cut off with a razor blade at the root base. Immediately, the pressure in the chamber was stepped up from 50 kPa to 500 kPa above atmosphere. The xylem sap exudated over a period of 10 min was collected. The rate of sap flow ($J = V/A_r \cdot t$) was determined by measuring sap volume per unit root area and per unit time. The surface area of the root (A_r) was measured using the WinRHIZO system (Regent Instruments Inc., <https://www.regentinstruments.com>). The Lp_r of individual samples was calculated from the slope of a plot of $J/(\Delta P + \sigma \Delta \Psi_s)$, where ΔP is the applied pressure, σ is the reflection coefficient for nutrient salts in the xylem, and $\Delta \Psi_s$ is the difference in osmotic potential between the exudated xylem sap and the root medium (hydroponic solution).

Investigation of plant phenotype and water use efficiency

The selected homologous T₂ seeds were germinated and grown under normal conditions, with a 12-h photoperiod (200 μmol m⁻² sec⁻¹) and with day/night temperatures of 30/22°C, respectively, in soil pots with regular irrigation in a growth chamber.

To investigate the effect of the overexpression of *OsPIP1;3* on the growth and development of the transgenic plants, the transgenic and WT plants were grown under equal conditions and their growth indexes, including plant size, and fresh and dry weights, were measured. One-month-old plantlets were used to measure WUE according to the method described by Wang *et al.* (2017b). The OX and the WT plantlets were grown in pots with SRWC maintained at 85%. The

pots were covered with foil to prevent water evaporation. Each pot was irrigated with equal volumes of water to achieve 85% SRWC every 4 days for a total of 32 days. Each plant was weighed and the WUE was calculated as follows:

$WUE = (FW_f - FW_i)/W_w$, where FW_i and FW_f are the fresh weights of each plantlet at 0 and 32 days, and W_w is the total water used for the 32 days.

Stomatal density was determined essentially by light microscopy of nail polish imprints taken from the top and bottom surfaces of the leaves. Total chlorophyll from tobacco leaves was extracted in 80% aqueous acetone and the contents were measured at wavelengths of 633 and 645 nm by spectrophotometry.

Gas exchange measurement and chlorophyll fluorescence

Fifty-day-old transgenic and WT tobacco plants growing in normal conditions were selected for the measurement of gas exchange and chlorophyll fluorescence (Flexas *et al.*, 2007, 2013b). The transpiration and photosynthesis rates of newly expanded leaves were measured using a 6400-40 Leaf Chamber Fluorometer (LICOR Biosciences, <https://www.licor.com>) under natural sunlight in the glasshouse. The CO_2 concentration in the cuvette was set at $400 \mu\text{mol mol}^{-1}$ with a CO_2 cartridge. The temperature of the leaf chamber was maintained at 25°C , with a photosynthetically active radiation of $1500 \mu\text{mol m}^{-2} \text{sec}^{-1}$. After equilibration to a steady state, the fluorescence was recorded (F_s) and a 0.8-sec saturating pulse of light (approximately $8000 \mu\text{mol m}^{-2} \text{sec}^{-1}$) was applied to measure the maximum fluorescence (F_m). The actual photochemical efficiency of photosystem II, $\Phi_{PSII} = (F_m - F_s)/F_m$, was used to calculate the electron transport rate ($J_{ETR} = \alpha \times PFD \times \Phi_{PSII}$), where α is a term including the product of leaf absorption and the partitioning of absorbed quanta between photosystems I and II, determined as the slope of the relationship between PSII and CO_2 obtained by varying light intensities under non-photorespiratory conditions in an atmosphere containing $<1\%$ O_2 , and PFD is the photosynthetically active photon flux density. The net photosynthetic rate (A_N), stomatal conductance (g_s), transpiration rate (T_r) and intercellular CO_2 concentration (C_i) were measured and calculated.

According to Harley *et al.* (1992), the leaf mesophyll conductance (g_m) was estimated using the equation: $g_m = A_N / (C_i - [\Gamma^* \times J_{ETR} + 8\Gamma^* (A_N + R_d)] / [J_{ETR} - 4(A_N + R_d)])$, where Γ^* represents a CO_2 compensation point without R_d . R_d is the rate of mitochondrial respiration in the light and was calculated using a linear regression line of the relationship between A_N and C_i for the range of C_i below $150 \mu\text{mol mol}^{-1}$. CO_2 concentration at the carboxylation sites in the stroma was calculated by using the g_m value obtained. Based on Fick's law of diffusion, the net photosynthetic flux (A_N) can be expressed as: $A_N = g_s (C_a - C_i) = g_m (C_i - C_c)$, where C_a is the CO_2 concentration in the atmosphere, C_i is the CO_2 concentration in the substomatal cavity and C_c is the chloroplast stroma, and can be calculated by the equation.

Measurement of plant resistance to water deficit

For drought tolerance treatment, young tobacco plants (2 months old) were grown in a growth chamber without irrigation for 6 days. Afterwards, the plants were then re-watered. The phenotypes were observed and recorded using photography. To measure the relative water content (RWC) of intact leaves on plants, representative leaves with a certain area size were collected before and after a 6-day drought treatment. To measure the RWC of the detached leaves, representative leaves of the same sizes and age

as described above were detached from the plants growing in normal conditions, and were weighed before and after air drying for 3 h. The water contents of all leaf samples were measured by comparing the weight differences before and after dehydration at 85°C for 1 h.

The relative water contents of intact leaves (RWC_i) and detached leaves (RWC_d) were calculated using the following equation:

$RWC = (FWW - DW_w)/(TFW - DW_t) \times 100\%$, where TFW is the fresh weight of turgid leaves, FWW is the fresh weights of wilted leaves after a 6-day drought (for intact leaves) or after 3 h of air drying (for detached leaves), DW_t is the dry weight of turgid leaves and DW_w is the dry weight of wilted leaves after a 6-day drought (for intact leaves) or after 3 h of air drying (for detached leaves).

The total soil water content was measured by determining soil weights before and after drying in an oven for 12–16 h at a temperature of 110°C . The SRWC was calculated using the following equation:

$SRWC = (W_a - W_d)/W_b - W_d \times 100\%$, where W_b is the soil weight before drought treatment, W_a is the soil weight after drought treatment and W_d is the soil weight after drying.

Functional analysis of OsPIP1;3 in cyanobacterium

Wild-type *Synechococcus* sp. PCC7942 cells (strain kindly provided by Dr Zhihan Lin, Institute of Oceanology, Chinese Academy of Sciences, China) were grown and maintained in liquid BG-11 medium (Ding *et al.*, 2013). The pSyn_1 vector for transformation of PCC7942 strain was purchased from Invitrogen (now ThermoFisher Scientific, <https://www.thermofisher.com>). The target gene with FLAG tag sequence was inserted into *HindIII* and *EcoRI* sites. The resulting construct or empty vector was transformed into cyanobacterial cells. The transformants were selected on solid BG-11 medium containing $50 \mu\text{g ml}^{-1}$ spectinomycin. To compare the growth rates, equal quantities of cells were dropped onto solid BG-11 media lacking $NaHCO_3$ and grown in normal air or CO_2 -free air, which was obtained by passing air through two CO_2 trap filters filled with NaOH and $Ca(OH)_2$. The air was supplied at 30 ml min^{-1} for 10 days at $50 \mu\text{mol photons m}^{-2} \text{sec}^{-1}$ of continuous illumination at 28°C . The cell growth patterns on solid media were photographed. Moreover, the cells were subjected to liquid culture and the cell densities (OD_{730}) were measured at the exponential phase.

Statistical data analysis

All experiments were carried out using biological duplications for each treatment, and were replicated on at least three occasions. Multiple-comparison tests were performed by Duncan's test using SPSS 16.0 (IBM, <https://www.ibm.com>). The significance level was set at $P < 0.05$.

ACKNOWLEDGEMENTS

We are thankful to Drs Mari Murai-Hatano and Atsuko Sakurai of the National Agricultural Research Center for Tohoku Region for providing us with anti-*OsPIP1;3* antibody, and to Dr Isao Shimamoto of the Nara Institute of Science and Technology for providing us with rice O.c. cells. This work was supported by the grants from National Natural Science Foundation of China (31670272) to X.D., the Natural Science Foundation of Heilongjiang province (C2017014) to X.D. and the Starting Fund of Northeast Agricultural University to X.D., and a grant from the Program for Promotion of Basic Research Activities for Innovative Biosciences (PROBRAIN, Japan) to Y.K. We thank Dr Victor Manon for his critical reading of this article.

AUTHOR CONTRIBUTIONS

XD, YK and GC designed this project; SL, TF, FP, QS and TM performed the gene cloning, protein expression, oocyte performance, immunoelectron microscopy, tobacco genetic transformation and characterization; PG and GC performed the stopped-flow work; MK and TK measured root hydraulic conductivity; SL, YZ, TF and QL performed the plant transgenic work and protein purification; SZ, WZ and AW performed the electrophysiology and biochemistry work; and XD, SL and GC wrote and revised the article.

CONFLICT OF INTEREST

The authors declare that there are no conflicts of interest to report.

OPEN RESEARCH BADGES



This article has earned an Open Data Badge for making publicly available the digitally shareable data necessary to reproduce the reported results.

This article has earned an Open Materials Badge for making publicly available the components of the research methodology needed to reproduce the reported procedure and analysis.

DATA AVAILABILITY STATEMENT

All relevant data can be found within the article and its supporting material.

SUPPORTING INFORMATION

Additional Supporting Information may be found in the online version of this article.

Figure S1. Alignment of OsPIP1;3 sequences from different rice varieties. OsPIP1;3in is from *Oryza sativa* L. *indica* cv. Zhonghan 3 and OsPIP1;3jp is from *Oryza sativa* L. *japonica* cv. Nipponbare. The isoleucine residues that are supposed to affect CO₂ permeability of plant AQPs are marked in the red box.

Figure S2. *In situ* localization of OsPIP1;3 in rice root. Rice root tips were fixed and subsequently embedded in 100 % LR-white. Ultrathin sections were prepared and immunostained with an anti-OsPIP1;3 specific rabbit antibody (a–c) or rabbit sera (d) and gold colloid labeled anti-rabbit IgG antibody. The samples were stained with Tl blue and observed by electron microscope.

Figure S3. Expression, solubilization and purification of OsPIP1;3 in the *E. coli* system. (a) Western blotting analysis using anti-OsPIP1;3 polyclonal antibody to detect solubilization efficiency by different detergents. Lanes 0 and 1 show the crude membrane fraction before and after being re-suspended in solubilization buffer (25 mM Na₂HPO₄, 10% (v/v) glycerol, 5 mM β-mercaptoethanol, and 125 mM NaCl, pH 8.0) without any detergent. Lanes 2–9 show the profiles of the proteins solubilized in solutions with 5% OG (lane 2), 10% OG (lane 3), 5% DM (lane 4), 5% C12E8 (lane 5), 5% OPOE (lane 6), 3% LDAO (lane 7), 1.5% FC12 (lane 8) and 4% PFO (lane 9), respectively. (b) Protein purification analysis. The

detergent-solubilized membrane proteins were separated by SDS-PAGE and stained with Coomassie brilliant blue (CBB) and then were subjected to Western blotting using anti-OsPIP1;3 polyclonal antibody. Loading profile: molecular weight marker (lane M), total PFO soluble membrane fraction (lane 1), the 1st passed fraction through the Ni-NTA column (lane 2), washing fraction (lane 3), and elution fraction (lane 4).

Figure S4. Expression of EGFP or EGFP-OsPIP1;3 in HEK293 cells. (a) Images of EGFP or EGFP-OsPIP1;3 in HEK293 cells. The arrow indicates the localization of EGFP-OsPIP1;3 in the membrane. (b) WB to show expression of EGFP or EGFP-OsPIP1;3.

Figure S5. Generation of OsPIP1;3 transgenic tobacco plants. (a) Schematic illustration of the T-DNA sequence of the pPBEL-FLAG-OsPIP1;3 construct. A FLAG tag sequence was inserted in the 5' of the *OsPIP1;3* gene to generate FLAG-OsPIP1;3 fusion protein for Western blotting. (b) Expression levels of *OsPIP1;3* and endogenous *NtAQP1* genes in tobacco plants. Total RNA was extracted from each T₂ plant and subject to RT-qPCR analyses.

Figure S6. Stomatal conductances (g_s) of OsPIP1;3 overexpression and wild-type plants. 50-day-old transgenic and WT tobacco plants growing in normal conditions were selected for gas exchange measurement. The indexes were measured with a 6400-40 Leaf Chamber Fluorometer (LICOR Biosciences) under natural sunlight in the glasshouse. See detailed description in the 'Experimental procedures'.

Figure S7. Transpiration rate (T_r) of OsPIP1;3 overexpression and WT plants. See the detailed description in 'Experimental procedures'.

Figure S8. Intercellular CO₂ concentration (C_i) of OsPIP1;3 overexpression and WT plants. See the detailed description in 'Experimental procedures'.

Figure S9. Total chlorophyll and nitrogen contents in tobacco leaves. (a) Total chlorophyll contents of wild-type and OX leaves. (b) Total nitrogen contents of WT and OX leaves.

Figure S10. Promotion of cyanobacterial growth by expression of *OsPIP1;3*. (a) FLAG-OsPIP1;3 expression in cyanobacteria revealed by Western blotting. (b) Growth patterns of transgenic and wild-type cells on solid medium exposed to CO₂-free or normal air. (c) The transgenic and wild-type cells were inoculated in liquid medium with equal density and were cultured in liquid medium in normal air. Their relative growth rates were measured and compared at the exponential growth phases.

Figure S11. Relative water content in pot soils. The plants were grown in pot soil with equal water contents. After a 6-day drought treatment, the pot soil water contents were measured. The values were the percentages of water contents after versus before the 6-day drought treatment.

Figure S12. Stomatal densities on WT and OsPIP1;3 transgenic leaves. The leaves from the top and bottom of representative WT and OsPIP1;3 transgenic plants were sampled. The stomatal densities were determined by means of nail polish imprints.

Figure S13. Pressure chamber for measuring root hydraulic conductance. Diagram of pressure chamber for measurement of root hydraulic conductance.

Figure S14. Effect of OsPIP1;3 overexpression on tobacco leaf area. One-month-old transgenic and WT tobacco plantlets were grown in pot soils. The pots were irrigated every 4 days for a total of 32 days. The first six true leaves were selected and the leaf areas were measured.

Table S1. Primer sequences for real-time RT-qPCR used to quantify gene expression levels.

REFERENCES

- Abascal, F., Irisarri, I. and Zardoya, R. (2014) Diversity and evolution of membrane intrinsic proteins. *Biochim. Biophys. Acta*, **1840**, 1468–1481.
- Aharon, R., Shahak, Y., Wininger, S., Bendov, R., Kapulnik, Y. and Galilia, G. (2003) Overexpression of a plasma membrane aquaporin in transgenic tobacco improves plant vigor under favorable growth conditions but not under drought or salt stress. *Plant Cell*, **15**, 439–447.
- Alexandersson, E., Frayssé, L., Sjövall-Larsen, S., Gustavsson, S., Fellert, M., Karlsson, M., Johanson, U. and Kjellbom, P. (2005) Whole gene family expression and drought stress regulation of aquaporins. *Plant Mol. Biol.* **59**, 469–484.
- Almeida-Rodríguez, A.M., Cooke, J.E.K., Yeh, F. and Zwiazek, J.J. (2010) Functional characterization of drought-responsive aquaporins in *Populus balsamifera* and *Populus simonii* × *balsamifera* clones with different drought resistance strategies. *Physiol. Plant.* **140**, 321–333.
- Baba, A., Hasezawa, S. and Syono, K. (1986) Cultivation of rice protoplasts and their transformation mediated by *Agrobacterium* spheroplasts. *Plant Cell Physiol.* **27**, 463–471.
- Bienert, M.D., Diehn, T.A., Richet, N., Chaumont, F. and Bienert, G.P. (2018) Heterotetramerization of plant PIP1 and PIP2 aquaporins is an evolutionary ancient feature to guide PIP1 plasma membrane localization and function. *Front. Plant Sci.* **9**, 382.
- Borgnia, M.J., Kozono, D., Calamita, G., Maloney, P.C. and Agre, P. (1999) Functional reconstitution and characterization of AqpZ, the *E. coli* water channel protein. *J. Mol. Biol.* **291**, 1169–1179.
- Calamita, G., Bishai, W.R., Preston, G.M., Guggino, W.B. and Agre, P. (1995) Molecular cloning and characterization of AqpZ, a water channel from *Escherichia coli*. *J. Biol. Chem.* **270**, 29063–29066.
- Calamita, G., Gena, P., Meleleo, D., Ferri, D. and Svelto, M. (2006) Water permeability of rat liver mitochondria: a biophysical study. *Biochim. Biophys. Acta-Biomembr.* **1758**, 1018–1024.
- Chaumont, F., Barrieu, F., Jung, R. and Chrispeels, M.J. (2000) Plasma membrane intrinsic proteins from maize cluster in two sequence subgroups with differential aquaporin activity. *Plant Physiol.* **122**, 1025–1034.
- Chevalier, A.S. and Chaumont, F. (2015) Trafficking of plant plasma membrane aquaporins: multiple regulation levels and complex sorting signals. *Plant Cell Physiol.* **56**, 819–829.
- Clarkson, D.T., Carvajal, M., Henzler, T., Waterhouse, R.N., Smyth, A.J., Cooke, D.T. and Steudle, E. (2000) Root hydraulic conductance: diurnal aquaporin expression and the effects of nutrient stress. *J. Exp. Bot.* **51**, 61–70.
- Crozet, P., Margalha, L., Confraria, A., Rodrigues, A., Martinho, C., Adamo, M., Elias, C.A. and Baena-González, E. (2014) Mechanisms of regulation of SNF1/AMPK/SnRK1 protein kinases. *Front. Plant Sci.* **5**, 190.
- Dean, R.M., Rivers, R.L., Zeidel, M.L. and Roberts, D.M. (1999) Purification and functional reconstitution of soybean nodulin 26. An aquaporin with water and glycerol transport properties. *Biochemistry*, **38**, 347–353.
- Deshmukh, R.K., Sonah, H. and Bélanger, R.R. (2016) Plant aquaporins: genome-wide identification, transcriptomics, proteomics, and advanced analytical tools. *Front. Plant Sci.* **7**, 1896.
- Ding, X., Iwasaki, I. and Kitagawa, Y. (2004) Overexpression of a lily PIP1 gene in tobacco increased the osmotic water permeability of leaf cells. *Plant Cell Environ.* **27**, 177–186.
- Ding, X., Matsumoto, T., Gena, P. et al. (2013) Water and CO₂ permeability of SsAqpZ, the cyanobacterium *Synechococcus* sp. PCC7942 aquaporin. *Biol. Cell*, **105**, 118–128.
- Echevarria, M., Windhager, E.E. and Frindt, G. (1996) Selectivity of the renal collecting duct water channel aquaporin-3. *J. Biol. Chem.* **271**, 25079–25082.
- Fetter, K., van Wilder, V., Moshelion, M. and Chaumont, F. (2004) Interactions between plasma membrane aquaporins modulate their water channel activity. *Plant Cell*, **16**, 215–228.
- Flexas, J., Ribas-Carbó, M., Hanson, D.T., Bota, J., Otto, B., Cifre, J., McDowell, N., Medrano, H. and Kaldenhoff, R. (2006) Tobacco aquaporin NtAQP1 is involved in mesophyll conductance to CO₂ *in vivo*. *Plant J.* **48**, 427–439.
- Flexas, J., Ortuño, M.F., Ribas-Carbo, M., Diaz-Espejo, A., Flórez-Sarasa, I.D. and Medrano, H. (2007) Mesophyll conductance to CO₂ in *Arabidopsis thaliana*. *New Phytol.* **175**, 501–511.
- Flexas, J., Niinemets, U., Gallé, A. et al. (2013a) Diffusional conductances to CO₂ as a target for increasing photosynthesis and photosynthetic water-use efficiency. *Photosynth Res.* **117**, 45–59.
- Flexas, J., Scoffoni, C., Gago, J. and Sack, L. (2013b) Leaf mesophyll conductance and leaf hydraulic conductance: an introduction to their measurement and coordination. *J. Exp. Bot.* **64**, 3965–3981.
- Fox, A.R., Maistriaux, L. and Chaumont, F. (2017) Towards understanding of the high number of plant aquaporin isoforms and multiple regulation mechanisms. *Plant Sci.* **264**, 179–187.
- Gaspar, M., Bousser, A., Sissoeff, I., Roche, O., Hoarau, J. and Mahe, A. (2003) Cloning and characterization of ZmPIP1-5b, an aquaporin transporting water and urea. *Plant Sci.* **165**, 21–31.
- Gena, P., Pellegrini-Calace, M., Biasco, A., Svelto, M. and Calamita, G. (2011) Aquaporin membrane channels: biophysics, classification, functions, and possible biotechnological applications. *Food Biophys.* **6**, 241–249.
- Gloser, V., Zwieniecki, M.A., Orians, C.M. and Holbrook, N.M. (2007) Dynamic changes in root hydraulic properties in response to nitrate availability. *J. Exp. Bot.* **58**, 2409–2415.
- Gronid, A., Mauleon, R., Vadez, V. and Henry, A. (2016) Root aquaporins contribute to whole plant water fluxes under drought stress in rice (*Oryza sativa* L.). *Plant Cell Environ.* **39**, 347–365.
- Groszmann, M., Osborn, H.L. and Evans, J.R. (2017) Carbon dioxide and water transport through plant aquaporins. *Plant Cell Environ.* **40**, 938–961.
- Hamill, O.P., Marty, A., Neher, E., Sakmann, B. and Sigworth, F.J. (1981) Improved patch-clamp techniques for high-resolution current recording from cells and cell-free membrane patches. *Pflugers Arch.* **391**, 85–100.
- Harley, P.C., Loreto, F., Marco, G.D. and Sharkey, T.D. (1992) Theoretical considerations when estimating the mesophyll conductance to CO₂ flux by analysis of the response of photosynthesis to CO₂. *Plant Physiol.* **98**, 1429–1436.
- Hedrich, R. and Geiger, D. (2017) Biology of SLAC1-type anion channels from nutrient uptake to stomatal closure. *New Phytol.* **216**, 46–61.
- van Heeswijk, M.P.E. and van Os, C.H. (1986) Osmotic water permeabilities of brush border and basolateral membrane vesicles from rat renal cortex and small intestine. *J. Membr. Biol.* **92**, 183–193.
- Hwang, J.H., Ellingson, S.R. and Roberts, D.M. (2010) Ammonia permeability of the soybean nodulin 26 channel. *FEBS Lett.* **584**, 4339–4343.
- Ikeda, M., Beitz, E., Kozono, D., Guggino, W.B., Agre, P. and Yasui, M. (2002) Characterization of aquaporin-6 as a nitrate channel in mammalian cells. Requirement of pore-lining residue threonine 63. *J. Biol. Chem.* **277**, 39873–39879.
- Ishibashi, K., Morishita, Y. and Tanaka, Y. (2017) The evolutionary aspects of aquaporin family. *Adv. Exp. Med. Biol.* **969**, 35–50.
- Jang, J.Y., Kim, D.G., Kim, Y.O., Kim, J.S. and Kang, H. (2004) An expression analysis of a gene family encoding plasma membrane aquaporins in response to abiotic stresses in *Arabidopsis thaliana*. *Plant Mol. Biol.* **54**, 713–725.
- Jozefkovicz, C., Rosi, P., Sigaut, L., Soto, G., Pietrasanta, L., Amodeo, G. and Alleve, K. (2013) Loop A is critical for the functional interaction of two *Beta vulgaris* PIP aquaporins. *PLoS ONE*, **8**, e57993.
- Kadam, S., Abrial, A., Dhanapal, A.P., Koester, R.P., Vermerris, W., Jose, S. and Fritsch, F.B. (2017) Characterization and regulation of aquaporin genes of sorghum (*Sorghum bicolor* (L.) Moench) in response to water-logging stress. *Front. Plant Sci.* **8**, 862.
- Kaldenhoff, R. and Fischer, M. (2006) Functional aquaporin diversity in plants. *Biochem. Biophys. Acta*, **1758**, 1134–1141.
- Kaldenhoff, R., Grote, K., Zhu, J.J. and Zimmermann, U. (1998) Significance of plasmalemma aquaporins for water-transport in *Arabidopsis thaliana*. *Plant J.* **14**, 121–128.
- Katsuhara, M., Akiyama, Y., Koshio, K., Shibasaki, M. and Kasamo, K. (2002) Functional analysis of water channels in barley roots. *Plant Cell Physiol.* **43**, 885–893.
- Kozono, D., Ding, X., Iwasaki, I., Meng, X., Kamagata, Y., Agre, P. and Kitagawa, Y. (2003) Functional expression and characterization of an archaean aquaporin. AqpM from *Methanothermobacter marburgensis*. *J. Biol. Chem.* **278**, 10649–10656.
- Li, G., Tillard, P., Gojon, A. and Maurel, C. (2016) Dual regulation of root hydraulic conductivity and plasma membrane aquaporins by plant

- nitrate accumulation and high-affinity nitrate transporter NRT2.1. *Plant Cell Physiol.* **57**, 733–742.
- Lian, H.L., Yu, X., Ye, Q., Ding, X., Kitagawa, Y., Kwak, S.S., Su, W.A. and Tang, Z.C. (2004) The role of aquaporin RWC3 in drought avoidance in rice. *Plant Cell Physiol.* **45**, 481–489.
- Lian, H.L., Yu, X., Lane, D., Sun, W.N., Tang, Z.C. and Su, W.A. (2006) Upland rice and lowland rice exhibited different PIP expression under water deficit and ABA treatment. *Cell Res.* **16**, 651–660.
- Liu, H.Y., Yu, X., Cui, D.Y., Sun, M.H., Sun, W.N., Tang, Z.C., Kwak, S.S. and Su, W.A. (2007) The role of water channel proteins and nitric oxide signaling in rice seed germination. *Cell Res.* **17**, 638–649.
- Liu, C., Fukumoto, T., Matsumoto, T. et al. (2013) Aquaporin OsPIP1;1 promotes rice salt resistance and seed germination. *Plant Physiol. Biochem.* **63**, 151–158.
- Matsumoto, T., Lian, H.L., Su, W.A., Tanaka, D., Liu, C., Iwasaki, I. and Kitagawa, Y. (2009) Role of the aquaporin PIP1 subfamily in the chilling tolerance of rice. *Plant Cell Physiol.* **50**, 216–229.
- Matsuo, N., Ozawa, K. and Mochizuki, T. (2009) Genotypic differences in root hydraulic conductance of rice (*Oryza sativa* L.) in response to water regimes. *Plant Soil*, **316**, 25–34.
- Maurel, C., Reizer, J., Schroeder, J.I. and Chrispeels, M.J. (1993) The vacuolar membrane protein gamma-TIP creates water specific channels in *Xenopus* oocytes. *EMBO J.* **12**, 2241–2247.
- Maurel, C., Verdoucq, L., Luu, D.-T. and Santoni, V. (2008) Plant aquaporins: membrane channels with multiple integrated functions. *Annu. Rev. Plant Biol.* **59**, 595–624.
- Maurel, C., Boursiac, Y., Luu, D.-T., Santoni, V., Shahzad, Z. and Verdoucq, L. (2015) Aquaporins in plants. *Physiol. Rev.* **95**, 1321–1358.
- Maurel, C., Verdoucq, L. and Rodrigues, O. (2016) Aquaporins and plant transpiration. *Plant Cell Environ.* **39**, 2580–2587.
- Missner, A., Kügler, P., Saporov, S.M., Sommer, K., Mathai, J.C., Zeidel, M.L. and Pohl, P. (2008) Carbon dioxide transport through membranes. *J. Biol. Chem.* **283**, 25340–25347.
- Mori, I.C., Rhee, J., Shibusaka, M., Sasano, S., Kaneko, T., Horie, T. and Katsuhara, M. (2014) CO₂ transport by PIP2 aquaporins of barley. *Plant Cell Physiol.* **55**, 251–257.
- Murai-Hatano, M., Kuwagata, T., Sakurai, J., Nonami, H., Ahamed, A., Nagasuga, K., Matsunami, T., Fukushi, K., Maeshima, M. and Okada, M. (2008) Effect of low root temperature on hydraulic conductivity of rice plants and the possible role of aquaporins. *Plant Cell Physiol.* **49**, 1294–1305.
- Nakhoul, N.L., Davis, B.A., Romero, M.F. and Boron, W.F. (1998) Effect of expressing the water channel aquaporin-1 on the CO₂ permeability of *Xenopus* oocytes. *Am. J. Physiol.* **43**, C543–C548.
- Nguyen, M.X., Moon, S. and Jung, K.-H. (2013) Genome-wide expression analysis of rice aquaporin genes and development of a functional gene network mediated by aquaporin expression in roots. *Planta*, **238**, 669–681.
- Preston, G.M., Carroll, T.P., Guggino, W.B. and Agre, P. (1992) Appearance of water channels in *Xenopus* oocytes expressing red cell CHIP28 protein. *Science*, **256**, 385–387.
- Qin, X. and Boron, W.F. (2013) Mutation of a single amino acid converts the human water channel aquaporin 5 into an anion channel. *Am. J. Physiol.* **305**, C663–C672.
- Rodrigues, O., Reshetnyak, G., Grondin, A., Saijo, Y., Leonhardt, N., Maurel, C. and Verdoucq, L. (2017) Aquaporins facilitate hydrogen peroxide entry into guard cells to mediate ABA- and pathogen-triggered stomatal closure. *Proc. Natl Acad. Sci. USA*, **114**, 9200–9205.
- Schäfer, N., Maierhofer, T., Herrmann, J. et al. (2018) A tandem amino acid residue motif in guard cell SLAC1 anion channel of grasses allows for the control of stomatal aperture by nitrate. *Curr. Biol.* **28**, 1370–1379.
- She, J., Guo, J., Chen, Q., Zeng, W., Jiang, Y. and Bai, X. (2018) Structural insights into the voltage and phospholipid activation of mammalian TPC1 channel. *Nature*, **556**, 130–134.
- Shen, J., Fu, J., Ma, J., Wang, X., Gao, C., Zhuang, C., Wan, J. and Jiang, L. (2014) Isolation, culture, and transient transformation of plant protoplasts. *Curr. Protoc. Cell Biol.* **63**, 2.8.1–17.
- Song, S., Xu, Y., Huang, D., Miao, H., Liu, J., Jia, C., Hu, W., Valarezo, A.V., Xu, B. and Jin, Z. (2018) Identification of a novel promoter from banana aquaporin family gene (MaTIP1;2) which responds to drought and salt stress in transgenic *Arabidopsis thaliana*. *Plant Physiol. Biochem.* **128**, 163–169.
- Song, Y., Zhang, H., You, H. et al. (2019) Identification of novel interactors and potential phosphorylation substrates of GsSnRK1 from wild soybean (*Glycine soja*). *Plant Cell Environ.* **42**, 145–157.
- Takano, J., Wada, M., Ludewig, U., Schaaf, G., Wirén, N. and Fujiwara, T. (2006) The *Arabidopsis* major intrinsic protein NIP5;1 is essential for efficient boron uptake and plant development under boron limitation. *Plant Cell*, **18**, 1498–1509.
- Uehlein, N., Lovisolo, C., Siefritz, F. and Kaldenhoff, R. (2003) The tobacco aquaporin NtAQP1 is a membrane CO₂ pore with physiological functions. *Nature*, **425**, 734–737.
- Vieira, P.M., Santos, M.P., Andrade, C.M., Souza-Neto, O.A., Ulhoa, C.J. and Aragão, F.J.L. (2017) Overexpression of an aquaglyceroporin gene from *Trichoderma harzianum* improves water-use efficiency and drought tolerance in *Nicotiana tabacum*. *Plant Physiol. Biochem.* **121**, 38–47.
- Wang, Y.H., Garvin, D.F. and Kochian, L.V. (2001) Nitrate-induced genes in tomato roots. Array analysis reveals novel genes that may play a role in nitrogen nutrition. *Plant Physiol.* **127**, 345–359.
- Wang, X., Cai, H., Li, Y., Zhu, Y., Ji, W., Bai, X., Zhu, D. and Sun, X. (2015) Ectopic overexpression of a novel *Glycine soja* stress-induced plasma membrane intrinsic protein increases sensitivity to salt and dehydration in transgenic *Arabidopsis thaliana* plants. *J. Plant Res.* **128**, 103–113.
- Wang, C., Hu, H., Qin, X., Zeise, B., Xu, D., Rappel, W.J., Boron, W.F. and Schroeder, J.I. (2016) Reconstitution of CO₂ regulation of SLAC1 anion channel and function of CO₂-permeable PIP2;1 aquaporin as CARBONIC ANHYDRASE4 interactor. *Plant Cell*, **28**, 568–582.
- Wang, L., Li, Q.-T., Lei, Q., Feng, C., Zheng, X., Zhou, F., Li, L., Liu, X. and Kong, J. (2017a) Ectopically expressing MdPIP1;3, an aquaporin gene, increased fruit size and enhanced drought tolerance of transgenic tomatoes. *BMC Plant Biol.* **17**, 246.
- Wang, L., Wang, S., Chen, W., Li, H. and Deng, X. (2017b) Physiological mechanisms contributing to increased water-use efficiency in winter wheat under organic fertilization. *PLoS ONE*, **12**, e0180205.
- Wu, F., Sheng, P., Tan, J. et al. (2015) Plasma membrane receptor-like kinase leaf panicle 2 acts downstream of the DROUGHT AND SALT TOLERANCE transcription factor to regulate drought sensitivity in rice. *J. Exp. Bot.* **66**, 271–281.
- Xu, F., Wang, K., Yuan, W. et al. (2019) Overexpression of rice aquaporin OsPIP1;2 improves yield by enhancing mesophyll CO₂ conductance and phloem sucrose transport. *J. Exp. Bot.* **70**, 671–681.
- Zhuo, C., Wang, T., Guo, Z. and Lu, S. (2016) Overexpression of MfPIP2-7 from *Medicago falcata* promotes cold tolerance and growth under NO₃⁻ deficit in transgenic tobacco plants. *BMC Plant Biol.* **16**, 138.
- Zwiak, J.J., Xu, H., Tan, X., Navarro-Ródenas, A. and Morte, A. (2017) Significance of oxygen transport through aquaporins. *Sci. Rep.* **7**, 40411.